5

THIN PLATES. KIRCHHOFF THEORY

5.1 INTRODUCTION

This chapter introduces the study of structures formed by "thin surfaces" such as plates and shells. Plates will be studied in this and the two following chapters. Shell structures formed by assembly of flat plates will be considered in Chapter 8. Axisymmetric shells will be treated in Chapter 9. Finally, the more general case of curved shell structures of arbitrary shape will be studied in Chapter 10.

Plate theory is a simplification of 3D elasticity analogous to that made in Chapters 1–3 for the analysis of beams, which serves as a solid foundation to what follows.

Like for beams, plate theories differ on the assumptions for the rotation of the normal to the middle plane. The classic thin plate theory establishes that the normal remains straight and orthogonal to the middle plane after deformation. Thin plate theory is based on the assumptions formalized by Kirchhoff in 1850 [Ki] and indeed his name is often associated with this theory, through an early version was proposed by Sophie Germain in 1811 [BD7,Re3,TW]. The more advanced thick plate theory proposed by Reissner [Re] and Mindlin [Mi] assumes that normals remain straight, though not necessarily orthogonal to the middle plane after deformation.

This chapter presents the formulation of plate elements following Kirchhoff thin plate theory. Like for Euler-Bernouilli beam elements, Kirchhoff plate elements require C^1 continuity of the deflection field due to the presence of second derivatives of the deflection in the virtual work expression. However, unlike beam elements, Kirchhoff plate elements have serious difficulties for satisfying the continuity requirements between elements. This leads to "non-conforming" elements, some of which can be still applied to practical situations.

E. Oñate, *Structural Analysis with the Finite Element Method. Linear Statics: Volume 2: Beams, Plates and Shells*, Lecture Notes on Numerical Methods in Engineering and Sciences, DOI 10.1007/978-1-4020-8743-1_5,

A part of this chapter studies rotation-free Kirchhoff plate elements with the deflection as the only nodal variable. These elements are an extension of the rotation-free beam elements studied in Chapter 1 and are competitive for many practical applications. Their formulation combines finite element and finite volume concepts.

Plate elements based on Reissner-Mindlin theory will be studied in the next chapter. These elements are analogous to Timoshenko beam elements and include the effect of shear deformation. This makes them applicable for both thick and thin situations and they require only C^0 continuity for the deflection. Reduced integration and equivalent procedures are necessary to avoid shear locking, like for slender Timoshenko beam elements.

Which of the plate theories is more appropiate? This is the logical question that an unexperienced reader would ask in order not to waste time studying concepts that may be of little use, or even obsolete. In answer, we would say that the study of both Kirchhoff and Reissner-Mindlin theories is highly recommended. Kirchhoff plate elements are available in most commercial codes and are continuously evolving due to the introduction of new concepts, such as the rotation-free formulation [OZ] and the isogeometric theory (Section 10.10 and [CHB]). Reissner-Mindlin plate elements, on the other hand, are attractive thanks to their versatility for analysis of thick and thin plates and the simplicity of their formulation. However, special care should be taken when using Reissner-Mindlin elements to avoid problems like shear locking or spureous mechanisms. In the next chapter we will show that some interesting thin plate elements can be derived by constraining the transverse shear strain to zero in Reissner-Mindlin elements.

5.2 KIRCHHOFF PLATE THEORY

5.2.1 Main assumptions

A plate is defined as a flat solid whose thickness is much smaller than its other dimensions. We assume that the *middle plane* is equidistant from the upper and lower faces. This plane is taken as the reference plane ($z = 0$) for deriving the plane kinematic equations. A plate with homogeneous isotropic material carries lateral loads by bending, like a straight beam (Figure 5.1). Hence the axial straining is zero, the middle plane coincides with the neutral plane and the displacement field can be expressed in terms of the lateral deflection and the rotations of the normal (the so called *bending*

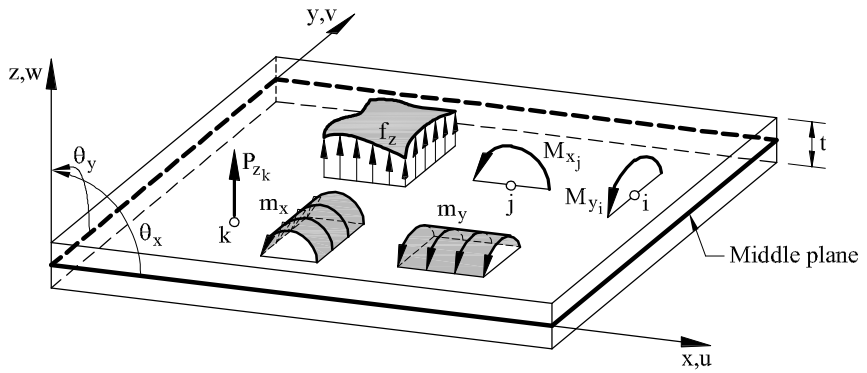

Fig. 5.1 Geometric definition of a plate. Sign convention for displacements, rotations, distributed and point loads and moments

state). If in-plane loading is present or the material is heterogeneous, the axial strains are not zero. This situation is studied in Chapters 7 and 8.

The assumptions of Kirchhoff thin plate theory are the following:

1. In the points belonging to the middle plane ($z = 0$)

$$u = v = 0 \tag{5.1}$$

   In other words, the points on the middle plane only move vertically.
2. The points along a normal to the middle plane have the same vertical displacement (i.e. the thickness does not change during deformation).
3. The normal stress σ_z is negligible (plane stress assumption).
4. A straight line normal to the undeformed middle plane *remains straight* and *normal* to the deformed middle plane (normal orthogonality condition).

Assumptions 1, 2 and 4 allow the displacement field to be defined over the whole plate. Assumption 3 affects the stress-strain relationship, as shown in Section 5.2.3.

5.2.2 Displacement field

From assumptions 1, 2, 4 and Figure 5.2, we deduce

$$\left.\begin{aligned} u(x,y,z) &= -z\theta_x(x,y) \\ v(x,y,z) &= -z\theta_y(x,y) \end{aligned}\right\} \text{(assumptions 1 and 4)}$$
$$w(x,y,z) = w(x,y) \qquad \text{(assumption 2)} \tag{5.2}$$

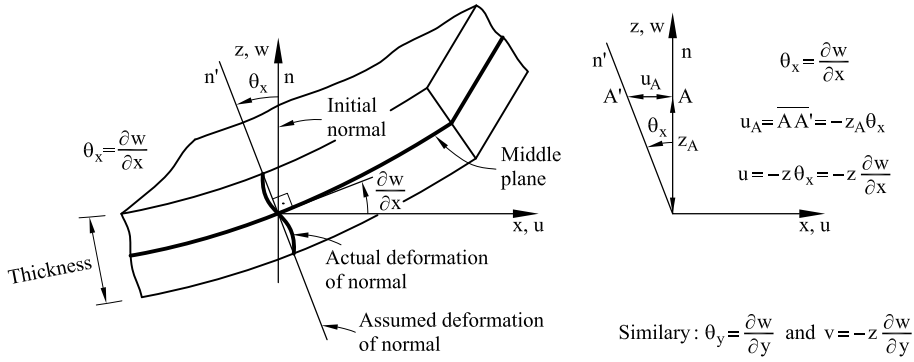

Fig. 5.2 Deformation of the normal vector and in-plane displacement field in a thin plate

where w is the vertical displacement (deflection) of the points on the middle plane and the rotations θ_x and θ_y coincide with the angles followed by the normal vectors contained in the planes xz and yz respectively in their motions (assumption 4). Vector

$$\mathbf{u} = [w, \theta_x, \theta_y]^T \tag{5.3}$$

is the *displacement vector* of a point on the middle plane of the plate. Note that $\mathbf{u}$ contains the deflection and the two rotations.

From assumption 4 and Figure 5.2 we deduce

$$\theta_x = \frac{\partial w}{\partial x} \quad , \quad \text{and similarly} \quad \theta_y = \frac{\partial w}{\partial y} \tag{5.4}$$

i.e. *the rotations of the normal coincide with the slopes of the middle plane* at each point.

The *displacement field* in a plate can thus be expressed as

$$\begin{aligned} u(x,y,z) &= -z\frac{\partial w(x,y)}{\partial x} \\ v(x,y,z) &= -z\frac{\partial w(x,y)}{\partial y} \\ w(x,y,z) &= w(x,y) \end{aligned} \tag{5.5}$$

The displacement vector is written as

$$\mathbf{u} = \left[w, \frac{\partial w}{\partial x}, \frac{\partial w}{\partial y}\right]^T \tag{5.6}$$

The assumption that the normals remain straight is only an approximation since in practice the normals are distorted as shown in Figure 5.2 and the angles θ_x and θ_y depend on the thickness coordinate. The hypothesis of a straight normal is equivalent to assuming an "average" uniform rotation for the normal, which obviously simplifies the kinematics.

The normal orthogonality condition only holds for thin plates (thickness/average side ratio: $t/L \leq 0.05$). For moderately thick ($0.05 \leq t/L < 0.10$) and very thick ($t/L \geq 0.10$) plates, the distortion of the normal during deformation increases. Reissner-Mindlin theory studied in the next chapter represents a better approximation to the actual deformation of the plate in these cases. If the distortion of the normal is large, as for thick slabs or for particular loading types or boundary conditions, then it is necessary to make use of 3D elasticity theory [On4].

5.2.3 Strain and stress fields and constitutive equation

Using the strain-displacement expressions from 3D elasticity [On4] and Eqs.(5.5) gives

$$\begin{aligned}
\varepsilon_x &= \frac{\partial u}{\partial x} = -z\frac{\partial^2 w}{\partial x^2} \\
\varepsilon_y &= \frac{\partial v}{\partial y} = -z\frac{\partial^2 w}{\partial y^2}; \quad \varepsilon_z = 0 \\
\gamma_{xy} &= \frac{\partial u}{\partial y} + \frac{\partial v}{\partial x} = -2z\frac{\partial^2 w}{\partial x \partial y} \\
\gamma_{xz} &= \frac{\partial w}{\partial x} + \frac{\partial u}{\partial z} = \frac{\partial w}{\partial x} - \frac{\partial w}{\partial x} = 0 \\
\gamma_{yz} &= \frac{\partial w}{\partial y} + \frac{\partial v}{\partial z} = \frac{\partial w}{\partial y} - \frac{\partial w}{\partial y} = 0
\end{aligned} \tag{5.7}$$

Eq.(5.7) shows that the normal orthogonality assumption leads to zero transverse shear strains γ_{xz} and γ_{yz}. Therefore, the transverse shear stresses do not contribute to the deformation work. This does not mean that these stresses are insignificant. They can be computed "a posteriori" using the equilibrium conditions as shown in a next section. Note also that the condition of vanishing normal strain ($\varepsilon_z = 0$) is redundant, as the normal stress σ_z vanishes due to plane stress assumption and, hence, the work performed by the normal strain σ_z is zero (i.e. $\sigma_z \varepsilon_z = 0$).

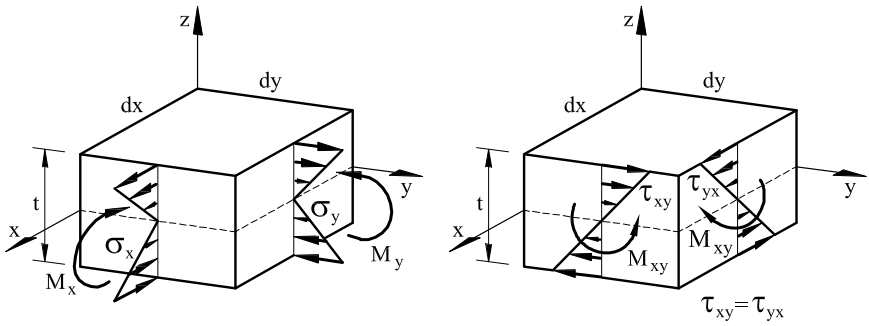

Fig. 5.3 Sign convention for stresses and bending moments

The strain vector containing the three significant strains is

$$\boldsymbol{\varepsilon} = \left[\varepsilon_x, \varepsilon_y, \gamma_{xy}\right]^T = \left[-z\frac{\partial^2 w}{\partial x^2}, -z\frac{\partial^2 w}{\partial y^2}, -2z\frac{\partial^2 w}{\partial x \partial y}\right]^T = \mathbf{S}\hat{\boldsymbol{\varepsilon}}_b \tag{5.8}$$

with

$$\mathbf{S} = -z\begin{bmatrix} 1\,0\,0 \\ 0\,1\,0 \\ 0\,0\,1 \end{bmatrix} = -z\mathbf{I}_3 \quad , \quad \hat{\boldsymbol{\varepsilon}}_b = \left[\frac{\partial^2 w}{\partial x^2}, \frac{\partial^2 w}{\partial y^2}, 2\frac{\partial^2 w}{\partial x \partial y}\right]^T \tag{5.9}$$

where $\hat{\boldsymbol{\varepsilon}}_b$ is the generalized strain vector (or *curvature vector*). Index b in $\hat{\boldsymbol{\varepsilon}}_b$ denotes the bending strains. Matrix $\mathbf{S}$ transforms the curvatures of the middle plane surface into the strains at any point across the thickness.

The strain vector is conjugate to the stress vector

$$\boldsymbol{\sigma} = \left[\sigma_x, \sigma_y, \tau_{xy}\right]^T \tag{5.10}$$

For sign convention, see Figure 5.3.

The constitutive relationship between stresses and strains is written in the standard form as

$$\boldsymbol{\sigma} = \mathbf{D}\boldsymbol{\varepsilon} \tag{5.11}$$

The constitutive matrix $\mathbf{D}$ is obtained from the general expression of 3D elasticity by introducing the plane stress assumption ($\sigma_z = 0$) and the conditions $\sigma_{xz} = \gamma_{yz} = 0$. The expression of $\mathbf{D}$ coincides with that of *plane stress* theory (Chapter 4 of [On4]) as the significative strains and stresses are the same in both cases. The general expression of $\mathbf{D}$ for an orthotropic material will be derived in Section 6.2.3. In this chapter we will consider *isotropic material* for simplicity. Hence,

$$\mathbf{D} = \frac{E}{1-\nu^2}\begin{bmatrix} 1 & \nu & 0 \\ \nu & 1 & 0 \\ 0 & 0 & \frac{1-\nu}{2} \end{bmatrix} \tag{5.12}$$

5.2.4 Bending moments and generalized constitutive matrix

The resultant stress vector (or bending moment vector) is defined as

$$\hat{\boldsymbol{\sigma}}_b = \begin{Bmatrix} M_x \\ M_y \\ M_{xy} \end{Bmatrix} = \int_{-\frac{t}{2}}^{+\frac{t}{2}} \mathbf{S}^T \begin{Bmatrix} \sigma_x \\ \sigma_y \\ \tau_{xy} \end{Bmatrix} dz = \int_{-\frac{t}{2}}^{+\frac{t}{2}} \mathbf{S}^T \boldsymbol{\sigma} dz \tag{5.13}$$

where M_x and M_y are the bending *moments* produced by the stresses σ_x and σ_y, respectively, and M_{xy} is the *torque* produced by the tangential stress τ_{xy}. The sign convention for the moments is shown in Figure 5.3. The signs of M_x and M_y are consistent with those of θ_x and θ_y, respectively. Also note that $\mathbf{S} \equiv \mathbf{S}^T$, as $\mathbf{S}$ is diagonal (Eq.(5.9)).

Substituting Eqs.(5.11) into (5.13) yields

$$\hat{\boldsymbol{\sigma}}_b = \int_{-\frac{t}{2}}^{+\frac{t}{2}} \mathbf{S}^T \mathbf{D} \boldsymbol{\varepsilon} dz = \int_{-\frac{t}{2}}^{+\frac{t}{2}} \mathbf{S}^T \mathbf{D} \mathbf{S} \hat{\boldsymbol{\varepsilon}}_b dz = \hat{\mathbf{D}}_b \, \hat{\boldsymbol{\varepsilon}}_b \tag{5.14}$$

The generalized bending constitutive matrix $\hat{\mathbf{D}}_b$ in Eq.(5.14) is obtained as

$$\hat{\mathbf{D}}_b = \int_{-\frac{t}{2}}^{+\frac{t}{2}} \mathbf{S}^T \mathbf{D} \mathbf{S} dz = \int_{-\frac{t}{2}}^{+\frac{t}{2}} z^2 \mathbf{D} dz \tag{5.15a}$$

For homogeneous material

$$\hat{\mathbf{D}}_b = \frac{t^3}{12} \mathbf{D} \tag{5.15b}$$

The principal bending moments M_I and M_{II} are the roots of the characteristic polynomial

$$\det[[M] - \lambda \mathbf{I}_2] = 0 \tag{5.16a}$$

where

$$[M] = \begin{bmatrix} M_x & M_{xy} \\ M_{xy} & M_y \end{bmatrix} \quad \text{and} \quad \mathbf{I}_2 = \begin{bmatrix} 1 & 0 \\ 0 & 1 \end{bmatrix} \tag{5.16b}$$

From Eq.(5.16a) we obtain

$$\begin{aligned} M_I &= \frac{M_x + M_y}{2} + \frac{1}{2}[(M_x - M_y)^2 + 4M_{xy}^2]^{1/2} \\ M_{II} &= \frac{M_x + M_y}{2} - \frac{1}{2}[(M_x - M_y)^2 + 4M_{xy}^2]^{1/2} \end{aligned} \tag{5.16c}$$

The sign for the principal bending moments is shown in Figure 5.4. The angle that the principal direction I forms with the x axis is obtained from

$$\text{tg}2\alpha = \frac{2M_{xy}}{M_x - M_y} \tag{5.16d}$$

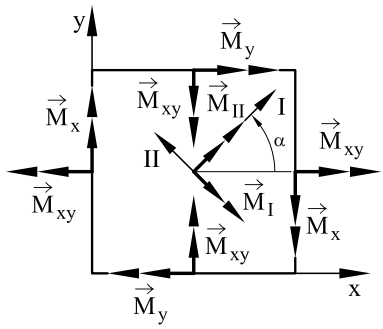

Fig. 5.4 Principal bending moments

5.2.5 Principle of virtual work

The PVW is written as

$$\iiint_V \delta\boldsymbol{\varepsilon}^T \boldsymbol{\sigma} dV = \iint_A \delta\mathbf{u}^T \mathbf{t} dA + \sum_i \delta\mathbf{u}_i^T \mathbf{p}_i \tag{5.17a}$$

with

$$\delta\mathbf{u} = \left[\delta w, \delta\left(\frac{\partial w}{\partial x}\right), \delta\left(\frac{\partial w}{\partial y}\right)\right]^T \quad , \quad \delta\mathbf{u}_i = \left[\delta w_i, \delta\left(\frac{\partial w}{\partial x}\right)_i, \delta\left(\frac{\partial w}{\partial y}\right)_i\right]^T$$
$$\mathbf{t} = [f_x, m_x, m_y]^T \quad , \quad \mathbf{p}_i = [P_{z_i}, M_{x_i}, M_{y_i}]^T \tag{5.17b}$$

In Eqs.(5.17), $\delta\mathbf{u}$ is the virtual displacement vector, $\mathbf{t}$ is the distributed force vector and $\mathbf{p}_i$ is the point force vector. As for the components of the load vectors, f_z is a distributed vertical force, m_x and m_y are distributed bending moments around the x and y axes, respectively, and F_{z_i}, M_{x_i} and M_{y_i} are the external vertical point load and the bending moments acting at point i, respectively (Figure 5.1). Moments are taken as positive if they act anticlockwise in the plane xz or yz (Figure 5.1).

The kinematic and constitutive expressions of the previous section allow us to simplify the virtual strain work δU given by the l. h. s. of Eq.(5.17a) into a surface integral over the plate middle plane (the "reference" geometry) in terms of the bending moments and the virtual curvatures. Making use of Eqs.(5.8) and (5.13) gives

$$\delta U = \iiint_V \delta\varepsilon^T \boldsymbol{\sigma} dV = \iiint_V \left[\mathbf{S}\delta\hat{\boldsymbol{\varepsilon}}_b^T\right]^T \boldsymbol{\sigma} dV =$$
$$= \iint_A \delta\hat{\boldsymbol{\varepsilon}}_b^T \left[\int_{-\frac{t}{2}}^{+\frac{t}{2}} \mathbf{S}^T \boldsymbol{\sigma} dz\right] dA = \iint_A \delta\hat{\boldsymbol{\varepsilon}}_b^T \hat{\boldsymbol{\sigma}}_b dA \tag{5.18}$$

Substituting Eq.(5.18) into (5.17a) gives the expression of the PVW as

$$\iint_A \delta\hat{\boldsymbol{\varepsilon}}_b^T \hat{\boldsymbol{\sigma}}_b dA = \iint_A \delta\mathbf{u}^T \mathbf{t} dA + \sum_i \delta\mathbf{u}_i^T \mathbf{p}_i \tag{5.19}$$

Consequently, *the plate can be treated as a 2D solid*, since all the variables and integrals in the PVW are functions of the coordinates of the middle plane only.

It is interesting to rewrite the expression of the virtual strain work of Eq.(5.18) as

$$\delta U = \iint_A \left[\frac{\partial^2 w}{\partial x^2} M_x + \frac{\partial^2 w}{\partial y^2} M_y + 2\frac{\partial^2 w}{\partial x \partial y} M_{xy} \right] dA \tag{5.20}$$

Eq.(5.20) clearly shows that the virtual strain work can be obtained as the integral over the plate area of the work performed by the bending moments over the corresponding virtual curvatures.

The integrand of (5.20) contains second derivatives of the deflection. This requires the continuity of the deflection and its first derivatives; i.e. C^1 continuity requirement (Section 3.8.3 of [On4]).

The C^1 continuity requirement for the deflection field is a particular feature of Kirchhoff plate elements, like it was for Euler-Bernouilli-beam elements (Chapter 1).

5.2.6 Equilibrium equations

The equilibrium equations are of particular interest in Kirchhoff plate theory. Among other things, they allow us to compute the shear forces from the nodal deflections. Also, the equilibrium equations have a simple differential form in terms of the deflection which has been widely used for the analytical (and numerical) solution of thin plate problems [TW].

The equilibrium of external forces, bending moments and shear forces over a differential element of a plate under distributed vertical forces f_z only (i.e. $m_x = m_y = 0$) (Figure 5.5) gives

Equilibrium of vertical forces

$$\sum F_z = o \quad \Rightarrow \quad \left(\frac{\partial Q_x}{\partial x} dx \right) dy + \left(\frac{\partial Q_y}{\partial y} dy \right) dx + f_z dx dy = 0 \tag{5.21a}$$

Dividing by the area differential ($dxdy$) gives

$$\frac{\partial Q_x}{\partial x} + \frac{\partial Q_y}{\partial y} + f_z = 0 \tag{5.21b}$$

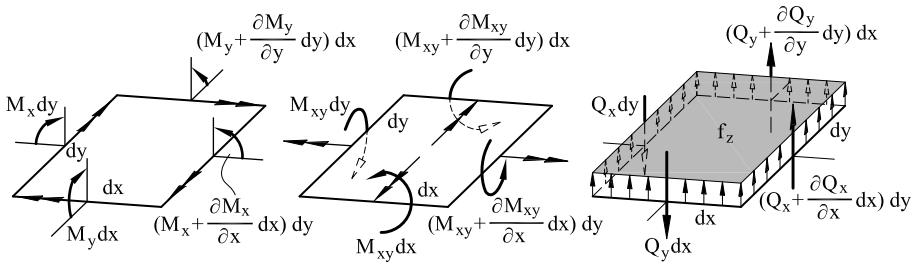

Fig. 5.5 Loads, moments and shear forces in a differential plate element

Equilibrium of moments

$$\sum M_x = 0 \quad \Rightarrow \quad \left(\frac{\partial M_x}{\partial x}dx\right)dy + \left(\frac{\partial M_{xy}}{\partial y}dy\right)dx + \\ + (Q_x dy)\,dx + \left(\frac{\partial Q_y}{\partial y}dy\right)dx\frac{dx}{2} - f_z dx dy\frac{dy}{2} = 0 \tag{5.22a}$$

$$\sum M_y = 0 \quad \Rightarrow \quad \left(\frac{\partial M_y}{\partial y}dy\right)dx + \left(\frac{\partial M_{xy}}{\partial x}dx\right)dy + \\ + (Q_y dx)dy + \left(\frac{\partial Q_x}{\partial x}dx\right)dy\frac{dy}{2} - f_z dx dy\frac{dy}{2} = 0 \tag{5.22b}$$

Ignoring second order terms we have after simplification

$$\frac{\partial M_x}{\partial x} + \frac{\partial M_{xy}}{\partial y} + Q_x = 0 \tag{5.23a}$$

$$\frac{\partial M_y}{\partial y} + \frac{\partial M_{xy}}{\partial x} + Q_y = 0 \tag{5.23b}$$

Differentiating Eqs.(5.23a) and (5.23b) with respect to y and x respectively, and substituting the derivatives of the shear forces into Eq.(5.21b) gives

$$\frac{\partial^2 M_x}{\partial x^2} + 2\frac{\partial^2 M_{xy}}{\partial x \partial y} + \frac{\partial^2 M_y}{\partial y^2} - f_z = 0 \tag{5.24}$$

Eq.(5.24) can be rewritten for an isotropic material using (5.14) as

$$\frac{\partial^4 w}{\partial x^4} + 2\frac{\partial^4 w}{\partial x^2 \partial y^2} + \frac{\partial^4 w}{\partial y^4} - \frac{f_z}{D} = 0 \tag{5.25a}$$

with

$$D = \frac{Et^3}{12(1-\nu^2)} \tag{5.25b}$$

Eq.(5.25a) is a fourth order differential equation relating the deflection to the applied distributed loading and the material properties of the plate.

Substituting Eq.(5.14) into (5.23) gives the expression for the shear forces in terms of the deflection as

$$Q_x = -D\left(\frac{\partial^3 w}{\partial x^3} + \frac{\partial^3 w}{\partial x \partial y^2}\right); \quad Q_y = -D\left(\frac{\partial^3 w}{\partial y^3} + \frac{\partial^3 w}{\partial y \partial x^2}\right) \tag{5.26}$$

The "exact" thickness distribution of the shear stresses can be found in terms of Q_x and Q_y from elasticity theory [Ug,VK,TW]. Accepting a parabolic distribution for the tangential stresses across the plate thickness, similarly as for beams, gives the maximum value of the shear stresses as [TW]

$$(\tau_{xz})_{\max} = \frac{3}{2}\frac{Q_x}{t}; \quad (\tau_{yz})_{\max} = \frac{3}{2}\frac{Q_y}{t} \tag{5.27}$$

5.2.7 The boundary conditions

The boundary conditions which have to be imposed on the problem are:

1. *Fixed boundary* where displacements at restrained points of the boundary are given specified values. These conditions are expressed as

$$w = \bar{w}\,,\ \theta_n = \bar{\theta}_n \text{ and } \theta_s = \bar{\theta}_s \tag{5.28}$$

Here n and s are directions normal and tangential to the boundary line (Figures 5.6 and 5.7) and $\bar{(\cdot)}$ denotes a prescribed value. Note that in Kirchhoff thin plate theory the specification of w along s automatically prescribes θ_s (as $\theta_s = \frac{\partial w}{\partial s}$, Figure 5.7b) but this is not the case for thick plates where w and θ_s are independently prescribed.

A *clamped edge* is a special case of Eq.(5.28) with zero values assigned to the prescribed values. A point support is characterized by $w_i = 0$ (Figure 5.7a).

2. *Traction boundary* where the resultant stresses M_n, M_{ns} and Q_n (Figure 5.6) are given prescribed values

$$M_n = \bar{M}_n \quad ; \quad M_{ns} = \bar{M}_{ns} \quad ; \quad Q_n = \bar{Q}_n \tag{5.29a}$$

The expressions for M_n, M_{ns} and Q_n can be obtained in terms of the bending moment and the shear forces as

$$M_n = M_x n_x^2 + 2M_{xy} n_x n_y + M_y n_y^2$$

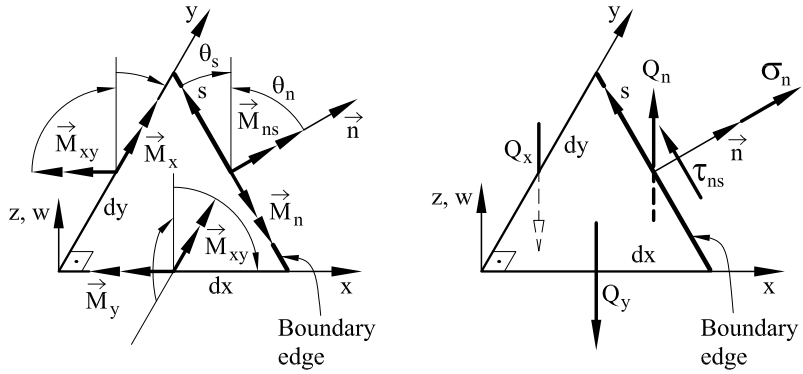

Fig. 5.6 Local rotations, local stresses and resultant stresses at a boundary edge

$$\begin{aligned} M_{ns} &= -M_x n_x n_y + M_{xy}(n_x^2 - n_y^2) + M_y n_x n_y \\ Q_n &= Q_x n_x + Q_y n_y \end{aligned} \tag{5.29b}$$

where n_x, n_y are the components of the unit normal vector $\mathbf{n} = [n_x, n_y]^T$ pointing towards the exterior of the boundary edge (Figure 5.6).

M_n and M_{ns} are the moments at the boundary edge induced by the normal stress σ_n and the tangential stress τ_{ns} at the edge obtained from

$$\begin{Bmatrix} \sigma_n \\ \tau_{ns} \end{Bmatrix} = \begin{bmatrix} n_x^2 & n_y^2 & 2n_x n_y \\ -n_x n_y & n_x n_y & (n_x^2 - n_y^2) \end{bmatrix} \begin{Bmatrix} \sigma_x \\ \sigma_y \\ \tau_{xy} \end{Bmatrix} \tag{5.29c}$$

Eq.(5.29c) can be deduced from the stress transformation given in Eq.(4.12b) of [On4]. For the sign of σ_n and τ_{ns} see Figure 5.6

The bending moments M_n and M_{ns} and the shear force Q_n are work-conjugate to the local rotations θ_n and θ_s and to the deflection w, respectively.

A *free edge* is a special case with zero values assigned to $\bar{M}_n, \bar{M}_{ns}$ and $\bar{\theta}_n$.

3. *Mixed boundary conditions*, where both traction and displacement components can be specified. A typical case is the *simply supported (SS) edge* (Figure 5.7b). Here it is clear that $w = 0$ (and consequently $\theta_s = 0$) and $M_n = 0$. It is less obvious whether $M_{ns} = 0$ needs to be specified. In practice it suffices to prescribe $w = 0$ at the nodes on the SS edge [ZT2]. For a curved SS edge modelled as a polynomial, a unique normal to each node must be specified and used to prescribe $w = \theta_s = 0$ at the node.

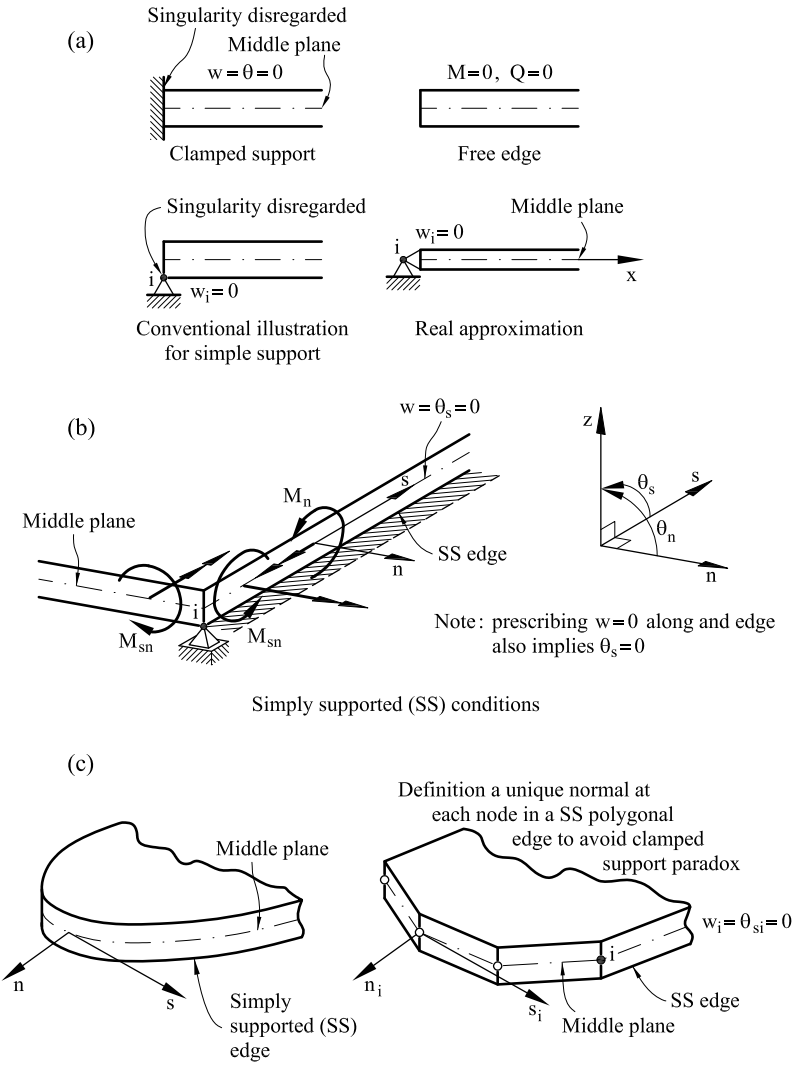

Fig. 5.7 (a) Supported (end) conditions for a plate. Conventionally illustrated simple support and real approximation. (b) Simply supported (SS) conditions. (c) Definition of unique normal and tangent directions in a SS polygonal edge

Otherwise the solution is equivalent, paradoxically, to that of a clamped support [Bab,BS].

The treatment of boundary conditions on edges which are inclined with respect to the cartesian axes is discussed in Section 6.3.5.

The alternatives for integrating the differential equations (5.25a) with the appropriate boundary conditions will not be discussed here. The more

popular analytical procedures are based on double Fourier series and the numerical ones on the finite difference method. Both techniques have been widely used to study a large variety of thin isotropic plates, generally of rectangular shape [Ga4,Pan,Sz,TW,Ug,VK].

The analytical study of thin plates with arbitrary geometry, heterogeneous material and complex boundary conditions is difficult. There are also severe limitations in the application of traditional numerical techniques such as the finite difference method.

The finite element method is free of most, if not all, the drawbacks mentioned above, as it can be easily applied to any plate problem, despite the complexity of the geometry or the material properties. It is interesting that it was in the solution of plate bending problems that the FEM gained its popularity in the late 1960's (see references in Chapter 11 of [ZT2]). The generality of the FEM versus the limitations of analytical solutions, or other numerical techniques, like grillage methods, and even the finite difference method, favoured the fast and broad development of the FEM for analysis of thin plates. Some of the more popular thin plate elements are described in the next sections.

5.3 FORMULATION OF THIN PLATE ELEMENTS

The intuitive way to satisfy the C^1 continuity requirement for the deflection is to choose the deflection and the two rotations as the nodal variables, in a similar way to what we do for Euler-Bernouilli beam elements.

Consequently, a thin plate element would have in principle three variables per node: w_i, $\left(\frac{\partial w}{\partial x}\right)_i$ and $\left(\frac{\partial w}{\partial y}\right)_i$, and the total number of variables for a n-noded element would be $3n$. This defines the number of polynomial terms approximating the deflection w within each element.

In general

$$w = \alpha_1 + \alpha_2 x + \alpha_3 y + \alpha_4 x^2 + \alpha_5 xy + ...(\text{up to } \ 3n \ \text{ terms}) \qquad (5.30)$$

The α_i parameters are obtained by imposing at each node

$$\left.\begin{aligned} & w_i = (w)_i \\ & \theta_{x_i} = \left(\frac{\partial w}{\partial x}\right)_i ; \quad \theta_{y_i} = \left(\frac{\partial w}{\partial y}\right)_i \end{aligned}\right\} \ i = 1, 2, ..., n \qquad (5.31)$$

which gives $3n$ equations.

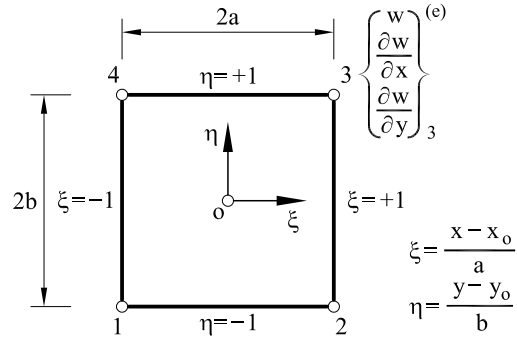

$$w = \sum_{i=1}^{4} [N_i w_i + \bar{N}_i (\frac{\partial w}{\partial x}) + \bar{\bar{N}}_i (\frac{\partial w}{\partial y})_i] \quad \begin{cases} N_i = (1+\xi_i\xi)(1+\eta_i\eta)(2+\xi_i\xi+\eta_i\eta-\xi^2-\eta^2)/8 \\ \bar{N}_i = a(\xi^2-1)(\xi+\xi_i)(1+\eta_i\eta)/8 \\ \bar{\bar{N}}_i = b(\eta^2-1)(\eta+\eta_i)(1+\xi_i\xi)/8 \end{cases}$$

$$\begin{array}{ccccccc} & & & 1 & & & \\ & & & \xi & & \eta & \\ & & \xi^2 & & \xi\eta & & \eta^2 \\ & \xi^3 & & \xi^2\eta & & \xi\eta^2 & & \eta^3 \\ \xi^4 & & \xi^3\eta & & \xi^2\eta^2 & & \xi\eta^3 & & \eta^4 \end{array}$$

Fig. 5.8 Non-conforming 4-noded MZC thin plate rectangle

The key issue is the selection of the adequate polynomial terms in Eq.(5.30) and, in general, several alternatives are possible. Each one defines a different plate element which performance must be carefully assesed since many of the elements just do not work in practice. In the following sections the pros and cons of some of the more popular rectangular and triangular Kirchhoff thin plate elements are presented.

5.4 RECTANGULAR THIN PLATE ELEMENTS

5.4.1 Non-conforming 4-noded MZC rectangle

The element is shown in Figure 5.8. It has four nodes and hence the number of polynomial terms in Eq.(5.30) is 12. It is however impossible to choose a complete polynomial for describing w, as the complete polynomials of third and quartic order have 10 and 15 terms, respectively (Figure 5.8). Thus, three terms of the quartic polynomial must be omitted. The

selection of these terms is not a trivial issue. Melosh [Me3] and Zienkiewicz and Cheung [ZCh,ZCh2] developed a popular 4-noded plate rectangle, denoted hereonwards MZC, on the basis of the following approximation

$$w = \alpha_1 + \alpha_2 x + \alpha_3 y + \alpha_4 x^2 + \alpha_5 xy + \alpha_6 y^2 + \alpha_7 x^3 + \alpha_8 x^2 y + \\ + \alpha_9 xy^2 + \alpha_{10} y^3 + \alpha_{11} x^3 y + \alpha_{12} xy^3 \tag{5.32}$$

Above expression guarantees geometry invariance [On4,ZTZ,ZT2]. Along the sides x =constant and y =constant the deflection varies as a complete third order polynomial which can be uniquely defined in terms of the two deflections and the two rotations at the end nodes of each side. This ensures the continuity of w between adjacent elements.

The $\alpha_1, \ldots, \alpha_{12}$ parameters are obtained making use of Eq.(5.31). It can be found after some algebra

$$\mathbf{a}^{(e)} = [w_1, \theta_{x_1}, \theta_{y_1}, \cdots, w_4, \theta_{x_4}, \theta_{y_4}] = \mathbf{A}\,[\alpha_1, \alpha_2, \alpha_3, \cdots, \alpha_{11}, \alpha_{12}]^T \tag{5.33a}$$

with

$$\mathbf{A} = \begin{bmatrix} 1 & x_1 & y_1 & x_1^2 & x_1 y_1 & y_1^2 & x_1^3 & x_1^2 y_1 & x_1 y_1^2 & y_1^3 & x_1^3 y_1 & x_1 y_1^3 \\ 0 & 1 & 0 & 2x_1 & y_1 & 0 & 3x_1^2 & 2x_1 y_1 & y_1^2 & 0 & 3x_1^2 y_1 & y_1^3 \\ 0 & 0 & 1 & 0 & x_1 & 2y_1 & 0 & x_1^2 & 2x_1 y_1 & 3y_1^2 & x_1^3 & 2x_1 y_1^2 \\ & & & \vdots & & & \vdots & & & \vdots & & \\ & & & \vdots & & & \vdots & & & \vdots & & \\ 0 & 0 & 1 & 0 & x_4 & 2y_4 & 0 & x_4^2 & 2x_4 y_4 & 3y_4^2 & x_4^3 & 2x_4 y_4^2 \end{bmatrix} \tag{5.33b}$$

Eq.(5.33a) gives

$$\boldsymbol{\alpha} = \mathbf{A}^{-1}\mathbf{a}^{(e)} \tag{5.34}$$

Combining Eqs.(5.32) and (5.34) yields, finally

$$w = \mathbf{P}^T\boldsymbol{\alpha} = \mathbf{P}^T\mathbf{A}^{-1}\mathbf{a}^{(e)} = \mathbf{N}\mathbf{a}^{(e)} \tag{5.35a}$$

where

$$\mathbf{N} = \mathbf{P}^T\mathbf{A}^{-1} \tag{5.35b}$$

is the shape function matrix with

$$\mathbf{P} = [1, x, y, x^2, xy, y^2, x^3, x^2 y, xy^2, y^3, x^3 y, xy^3]^T \tag{5.35c}$$

This process is quite tedious and costly. Melosh [Me3] derived an explicit form for the shape functions. Eq. (5.32) is rewritten as

$$w = \sum_{i=1}^{4} \left[N_i w_i + \bar{N}_i \left(\frac{\partial w}{\partial x} \right)_i + \bar{\bar{N}}_i \left(\frac{\partial w}{\partial y} \right)_i \right] = \mathbf{N}\mathbf{a}^{(e)} \tag{5.36}$$

where

$$\mathbf{N} = [\mathbf{N}_1, \mathbf{N}_2, \mathbf{N}_3, \mathbf{N}_4] \qquad ; \qquad \mathbf{a}^{(e)} = \begin{Bmatrix} \mathbf{a}_1^{(e)} \\ \mathbf{a}_2^{(e)} \\ \mathbf{a}_3^{(e)} \\ \mathbf{a}_4^{(e)} \end{Bmatrix} \tag{5.37}$$

and

$$\mathbf{N}_i = [N_i, \bar{N}_i, \bar{\bar{N}}_i] \qquad ; \qquad \mathbf{a}_i^{(e)} = \left[w_i, \left(\frac{\partial w}{\partial x} \right)_i, \left(\frac{\partial w}{\partial y} \right)_i \right]^T$$

Figure 5.8 shows the analytical form of the shape functions N_i, $\bar{N}_i$ and $\bar{\bar{N}}_i$ in natural coordinates. Similarly, as for the Hermite shape functions of the analogous 2-noded Euler-Bernouilli beam element (Eq.(1.11a)) function N_i corresponding to the deflection takes a unit value at node i, whereas its first derivatives are zero at the node. Conversely, functions $\bar{N}_i$ and $\bar{\bar{N}}_i$ have a zero value and unit slopes in the directions ξ and η, respectively at node i.

The curvature matrix is obtained from Eqs.(5.9) and (5.36) as

$$\hat{\boldsymbol{\varepsilon}}_b = \begin{Bmatrix} \dfrac{\partial^2 w}{\partial x^2} \\ \dfrac{\partial^2 w}{\partial y^2} \\ 2\dfrac{\partial^2 w}{\partial x \partial y} \end{Bmatrix} = \sum_{i=1}^{4} \mathbf{B}_{b_i} \mathbf{a}_i^{(e)} = \mathbf{B}_b \mathbf{a}^{(e)} \tag{5.38}$$

with

$$\mathbf{B}_b = [\mathbf{B}_{b_1}, \mathbf{B}_{b_2}, \mathbf{B}_{b_3}, \mathbf{B}_{b_4}] \quad , \quad \mathbf{B}_{b_i} = \begin{bmatrix} \dfrac{\partial^2 N_i}{\partial x^2} & \dfrac{\partial^2 \bar{N}_i}{\partial x^2} & \dfrac{\partial^2 \bar{\bar{N}}_i}{\partial x^2} \\ \dfrac{\partial^2 N_i}{\partial y^2} & \dfrac{\partial^2 \bar{N}_i}{\partial y^2} & \dfrac{\partial^2 \bar{\bar{N}}_i}{\partial y^2} \\ 2\dfrac{\partial^2 N_i}{\partial x \partial y} & 2\dfrac{\partial^2 \bar{N}_i}{\partial x \partial y} & 2\dfrac{\partial^2 \bar{\bar{N}}_i}{\partial x \partial y} \end{bmatrix} \tag{5.39}$$

The computation of the second derivatives of the shape functions in $\mathbf{B}_{b_i}$ is immediate simply noting that

$$\frac{\partial^2}{\partial x^2} = \frac{1}{a^2}\frac{\partial^2}{\partial \xi^2} \qquad \text{and} \qquad \frac{\partial^2}{\partial y^2} = \frac{1}{b^2}\frac{\partial^2}{\partial \eta^2} \tag{5.40}$$

The bending moment field is expressed in terms of the nodal DOFs by substituting Eq.(5.38) into (5.14). This gives

$$\hat{\boldsymbol{\sigma}}_b = \hat{\mathbf{D}}_b \mathbf{B}_b \mathbf{a}^{(e)} \tag{5.41}$$

It is deduced from Eqs.(5.35c) and (5.39) that the curvature field, and hence the bending moment field, is linear within the MZC element.

Following the usual procedure it is deduced that

$$\delta w = \mathbf{N}\delta\mathbf{a}^{(e)} \qquad \text{and} \qquad \delta\hat{\boldsymbol{\varepsilon}}_b = \mathbf{B}_b \delta\mathbf{a}^{(e)} \tag{5.42}$$

The PVW for a single element can be written as (see Eq.(5.19))

$$\iint_{A^{(e)}} \delta\hat{\boldsymbol{\varepsilon}}_b^T \hat{\boldsymbol{\sigma}}_b dA = \iint_{A^{(e)}} \delta\mathbf{u}^T \mathbf{t} dA + \sum_{i=1}^{3} [\delta\mathbf{a}_i^{(e)}]^T \mathbf{q}_i^{(e)} \tag{5.43a}$$

with

$$\delta\mathbf{a}_i^{(e)} = \left[\delta w_i, \delta\left(\frac{\partial w}{\partial x}\right)_i, \delta\left(\frac{\partial w}{\partial y}\right)_i\right]^T \quad , \quad \mathbf{q}_i^{(e)} = [F_{z_i}, M_{x_i}, M_{y_i}]^T \tag{5.43b}$$

where $\mathbf{q}_i^{(e)}$ is the vector of equilibrating nodal forces for node i.

Substituting Eqs.(5.42) and the constitutive equation (5.41) into the PWV, the standard equilibrium equation for the element is found as

$$\mathbf{K}^{(e)}\mathbf{a}^{(e)} - \mathbf{f}^{(e)} = \mathbf{q}^{(e)} \tag{5.44}$$

The element stiffness matrix is

$$\mathbf{K}_{ij}^{(e)} = \iint_{A^{(e)}} \mathbf{B}_{b_i}^T \hat{\mathbf{D}}_b \mathbf{B}_{b_j} dxdy \tag{5.45}$$

The equivalent nodal force vector for a distributed vertical loading and distributed bending moments is

$$\mathbf{f}_i^{(e)} = \begin{Bmatrix} f_{z_i} \\ m_{x_i} \\ m_{y_i} \end{Bmatrix} = \iint_{A^{(e)}} \begin{bmatrix} N_i & N_{i,x} & N_{i,y} \\ \bar{N}_i, & \bar{N}_{i,x} & \bar{N}_{i,y} \\ \bar{\bar{N}}_i & \bar{\bar{N}}_{i,x} & \bar{\bar{N}}_{i,y} \end{bmatrix} \begin{Bmatrix} f_z \\ m_x \\ m_y \end{Bmatrix} dxdy \tag{5.46}$$

$$\mathbf{K}^{(e)} = D\,[\mathbf{K}_1^{(e)} + \mathbf{K}_2^{(e)} + \mathbf{K}_3^{(e)} + \mathbf{K}_4^{(e)}] \qquad ; \qquad D = \frac{Et^3}{12(1-\nu^2)}$$

$$\mathbf{K}_1^{(e)} = \frac{b}{6a^3}\begin{bmatrix}
6 & & & & & & & & & & & \\
6a & 8a^2 & & & & & & & & & & \\
0 & 0 & 0 & & & & & & & & & \\
-6 & -6a & 0 & 6 & & & & & & & & \\
6a & 4a^2 & 0 & -6a & 8a^2 & & & \text{Symmetric} & & & & \\
0 & 0 & 0 & 0 & 0 & 0 & & & & & & \\
-3 & -3a & 0 & 3 & -3a & 0 & 6 & & & & & \\
3a & 2a^2 & 0 & -3a & 4a^2 & 0 & -6a & 8a^2 & & & & \\
0 & 0 & 0 & 0 & 0 & 0 & 0 & 0 & 0 & & & \\
3 & 3a & 0 & -3 & 3a & 0 & -6 & 6a & 0 & 6 & & \\
3a & 4a^2 & 0 & -3a & 2a^2 & 0 & -6a & 4a^2 & 0 & 6a & 8a^2 & \\
0 & 0 & 0 & 0 & 0 & 0 & 0 & 0 & 0 & 0 & 0 & 0
\end{bmatrix}$$

$$\mathbf{K}_2^{(e)} = \frac{a}{6b^3}\begin{bmatrix}
6 & & & & & & & & & & & \\
0 & 0 & & & & & & & & & & \\
6b & 0 & 8b^2 & & & & & & & & & \\
3 & 0 & 3b & 6 & & & & & & & & \\
0 & 0 & 0 & 0 & 0 & & & \text{Symmetric} & & & & \\
3b & 0 & 4b^2 & 6b & 0 & 8b^2 & & & & & & \\
-3 & 0 & -3b & -6 & 0 & -6b & 6 & & & & & \\
0 & 0 & 0 & 0 & 0 & 0 & 0 & 0 & & & & \\
3b & 0 & 2b^2 & 6b & 0 & 4b^2 & -6b & 0 & 8b^2 & & & \\
-6 & 0 & -6b & -3 & 0 & -3b & 3 & 0 & -3b & 6 & & \\
0 & 0 & 0 & 0 & 0 & 0 & 0 & 0 & 0 & 0 & 0 & \\
6b & 0 & 4b^2 & 3b & 0 & 2b^2 & -3b & 0 & 4b^2 & -6b & 0 & 8b^2
\end{bmatrix}$$

$$\mathbf{K}_3^{(e)} = \frac{\nu}{2ab}\begin{bmatrix}
1 & & & & & & & & & & & \\
a & 0 & & & & & & & & & & \\
b & 2ab & 0 & & & & & & & & & \\
-1 & 0 & -b & 1 & & & & & & & & \\
0 & 0 & 0 & -a & 0 & & & \text{Symmetric} & & & & \\
-b & 0 & 0 & b & -2ab & 0 & & & & & & \\
1 & 0 & 0 & -1 & a & 0 & 1 & & & & & \\
0 & 0 & 0 & a & 0 & 0 & -a & 0 & & & & \\
0 & 0 & 0 & 0 & 0 & 0 & -b & 2ab & 0 & & & \\
-1 & -a & 0 & 1 & 0 & 0 & -1 & 0 & b & 1 & & \\
-a & 0 & 0 & 0 & 0 & 0 & 0 & 0 & 0 & a & 0 & \\
0 & 0 & 0 & 0 & 0 & 0 & 0 & 0 & 0 & -b & -2ab & 0
\end{bmatrix}$$

$$\mathbf{K}_4^{(e)} = \frac{1-\nu}{30ab}\begin{bmatrix}
21 & & & & & & & & & & & \\
3a & 8a^2 & & & & & & & & & & \\
3b & 0 & 8b^2 & & & & & & & & & \\
-21 & -3a & -3b & 21 & & & & & & & & \\
3a & -2a^2 & 0 & -3a & 8a^2 & & & \text{Symmetric} & & & & \\
-3b & 0 & -8b^2 & 3b & 0 & 8b^2 & & & & & & \\
21 & 3a & 3b & -21 & 3a & -3b & 21 & & & & & \\
-3a & 2a^2 & 0 & 3a & -8a^2 & 0 & -3a & 8a^2 & & & & \\
-3b & 0 & 2b^2 & 3b & 0 & -2b^2 & -3b & 0 & 8b^2 & & & \\
-21 & -3a & -3b & 21 & -3a & 3b & -21 & 3a & 3b & 21 & & \\
-3a & -2a^2 & 0 & 3a & 2a^2 & 0 & -3a & -2a^2 & 0 & 3a & 8a^2 & \\
3b & 0 & -8b^2 & -3b & 0 & 2b^2 & 3b & 0 & -8b^2 & -3b & 0 & 8b^2
\end{bmatrix}$$

Box 5.1. 4-noded MZC thin plate rectangle ($2a \times 2b$). Stiffness matrix for homogeneous isotropic material

$$\hat{\boldsymbol{\sigma}}_b = \begin{Bmatrix} M_x \\ M_y \\ M_{xy} \end{Bmatrix} = \sum_{i=1}^{4} \hat{\mathbf{D}}_b \; \mathbf{B}_{b_i} \; \mathbf{a}_i^{(e)}$$

$$\hat{\mathbf{D}}_b \mathbf{B}_{b_i} = \begin{bmatrix} (\hat{d}_{11} \; N_i^{xx} + \hat{d}_{12} \; N_i^{yy}) & \hat{d}_{12} \; \bar{N}_i^{xx} & \hat{d}_{11} \; \bar{\bar{N}}_i^{yy} \\ (\hat{d}_{21} \; N_i^{xx} + \hat{d}_{22} \; N_i^{yy}) & \hat{d}_{21} \; \bar{N}_i^{xx} & \hat{d}_{22} \; \bar{\bar{N}}_i^{yy} \\ 2\hat{d}_{33} \; N_i^{xy} & 2\hat{d}_{33} \; \bar{N}_i^{xy} & 2\hat{d}_{33} \; \bar{\bar{N}}_i^{xy} \end{bmatrix}$$

$$N_i^{xx} = -\frac{1}{4a^2}(3\xi_i\xi + 3\xi_i\eta_i\xi\eta) \qquad \bar{N}_i^{xx} = \frac{1}{4a}(3\xi + \xi_i\eta_i\eta + 3\eta_i\xi\eta + \xi_i)$$

$$N_i^{yy} = -\frac{1}{4b^2}(3\eta_i\eta + 3\xi_i\eta_i\xi\eta) \qquad \bar{N}_i^{xy} = \frac{1}{8b}(3\eta_i\xi^2 + 2\xi_i\eta_i\xi - \eta_i)$$

$$N_i^{xy} = \frac{1}{8ab}(4\xi_i\eta_i - 3\xi_i\eta_i\xi^2 - 3\xi_i\eta_i\eta^2) \qquad \bar{\bar{N}}_i^{yy} = \frac{1}{4b}(3\eta + \xi_i\eta_i\xi + 3\xi_i\xi\eta + \eta_i)$$

$$\bar{\bar{N}}_i^{xy} = \frac{1}{8a}(3\xi_i\eta^2 + 2\xi_i\eta_i\eta - \xi)$$

$\hat{d}_{ij}$ term ij of matrix $\hat{\mathbf{D}}_b$

Box 5.2. 4-noded MZC thin plate rectangle. Matrix $\hat{\mathbf{D}}\mathbf{B}_{b_i}$ for computing the bending moments

where f_{z_i} , m_{x_i} and m_{y_i} are the vertical force and the bending moments acting at node i and $N_{i,x} = \frac{\partial N_i}{\partial x}$, etc.

Note that a distributed vertical loading originates nodal bending moments, like for Euler-Bernouilli beam elements. Similarly, distributed bending moments give nodal vertical forces. This is due to the dependence of the deflection field with the nodal rotations (Eq.(5.36)).

The integrals in Eqs.(5.45) and (5.46) can be computed numerically by a Gauss quadrature [On4]. However, the exact integration of the MZC rectangular element stiffness matrix is straightforward and its expression is given in Box 5.1 for homogeneous isotropic material. Box 5.2 shows the explicit product $\hat{\mathbf{D}}_b\mathbf{B}_i$ needed for computing the bending moment field via Eq.(5.41). The equivalent nodal force vector for a uniformly distributed vertical load $f_z = q$ is

$$\mathbf{f}^{(e)} = 4qab\left[\frac{1}{4}, \frac{a}{12}, \frac{b}{12}, \frac{1}{4}, -\frac{a}{12}, \frac{b}{12}, \frac{1}{4}, -\frac{a}{12}, -\frac{b}{12}, \frac{1}{4}, \frac{a}{12}, -\frac{b}{12}\right]^T \tag{5.47a}$$

The expression of $\mathbf{f}_i$ for external forces acting at a node is

$$\mathbf{f}_i = [P_{z_i}, M_{x_i}, M_{y_i}]^T \tag{5.47b}$$

where P_{z_i}, M_{x_i} and M_{y_i} are the vertical point load and the bending moments acting at node i, respectively (Figure 5.1).

The global system of equations $\mathbf{Ka} = \mathbf{f}$ is obtained by assembling the element stiffness matrices and equivalent nodal force vectors in the standard manner. Reactions at the prescribed nodes are computed a posteriori as explained in Section 1.3.4 for beams.

Example 5.1: Derive the term 11 of $\mathbf{K}_{11}^{(e)}$ for the MZC thin plate rectangle.

- Solution

From Eq.(5.45) we deduce

$$[\mathbf{K}_{ij}^{(e)}]_{11} = \iint_{A^{(e)}} [\mathbf{B}_{b_i}^T]_1 \ \hat{\mathbf{D}}_b [\mathbf{B}_{b_j}]_1 \ dxdy$$

where index 1 in $\mathbf{B}_i$ denotes the first row and in $\mathbf{B}_j$ the first column. Using Eqs.(5.39) and (5.40) and the expressions of Figure 5.8 we obtain

$$\begin{aligned}[\mathbf{K}_{ij}^{(e)}]_{11} = \int_{-1}^{+1}\int_{-1}^{+1} \Big[& 9\ \hat{d}_{11}\ b^4(1-\eta_j\eta)(1+\eta_i\eta)\xi_i\xi_j\xi^2 + \\ & +18 d_{12}\ a^2\ b^2\left((1+\eta_i\eta)(1+\xi_j\eta)\xi_i\eta_j\xi\eta + (1+\xi_i\xi)(1+\eta_j\eta)\eta_i\xi_j\xi\eta\right) + \\ & +a\ \hat{d}_{22}\ a^4(1+\xi_i\xi)(1+\xi_j\xi)\eta_i\eta_j\eta^2 + \hat{d}_{33}\ a^2\ b^2(3\xi^2+3\eta^2-4)\xi_i\eta_i\xi_j\eta_j \Big]\ a\ b\ d\xi\ d\eta\end{aligned}$$

where $\hat{d}_{ij}$ is the term ij of matrix $\hat{\mathbf{D}}_b$ in Eq.(5.15a). Integration gives

$$\begin{aligned}[\mathbf{K}_{ij}^{(e)}]_{11} = \frac{1}{4a^2b^2}\Big[& 3\ \hat{d}_{11}\ b^4\xi_i\xi_j(1+\frac{1}{3}\eta_i\eta_j) + 3\ \hat{d}_{22}\ a^4\eta_i\eta_j(1+\frac{1}{3}\xi_i\xi_j) + \\ & +2d_{12}\ a^2\ b^2\xi_i\xi_j\eta_i\eta_j + \frac{28}{5}\hat{d}_{33}\ a^2\ b^2\xi_i\xi_j\eta_i\eta_j\Big]\end{aligned}$$

Particularizing for $i = j = 1$ yields

$$[\mathbf{K}_{11}^{(e)}]_{11} = \hat{d}_{11}\frac{b}{a^3} + \hat{d}_{22}\ \frac{a}{b^3} + \frac{\hat{d}_{12}}{2\ ab} + \frac{7}{5}\frac{\hat{d}_{33}}{ab}$$

The same procedure yields the rest of stiffness matrix terms of Box 5.1.

Incompatibility of the normal rotation

It is important to understand that even though the deflection field of Eq.(5.36) guarantees the continuity of w between elements, however *it does not guarantee the continuity of the first derivatives of w (slopes)*, except at the nodes where it is obvious that they are uniquely defined. To

$$w^{(A)}=0 \qquad \left(\frac{\partial w}{\partial y}\right)^{(A)}=0$$

$$w^{(B)}=(\xi^2-1)(\xi-1)(1+\eta)/8 \qquad \left(\frac{\partial w}{\partial y}\right)^{(B)}=\left(\frac{\partial w}{\partial \eta}\ \frac{\partial \eta}{\partial y}\right)^{(B)}=\frac{l_{25}}{2}(\xi^2-1)(\xi-1)/8$$

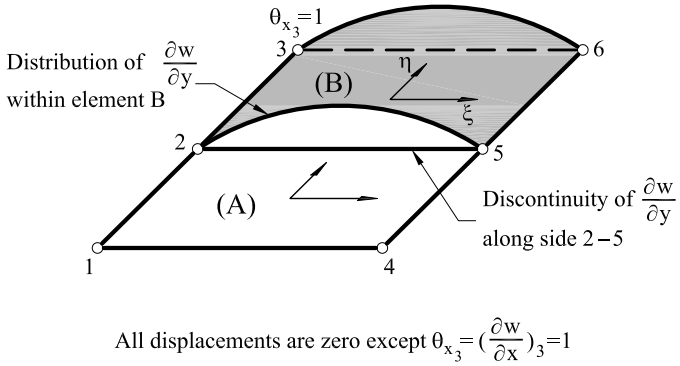

Fig. 5.9 Discontinuity of the slope $\frac{\partial w}{\partial y}$ along a side of a 4-noded rectangular plate

clarify this, let us consider the two elements A and B of Figure 5.9. It is assumed that all the nodal variables are zero with the exception of $\theta_{x_3} = 1$. Since $w = 0$ over element 1, then $\left(\frac{\partial w}{\partial y}\right) = 0$ along side 2-5 shared by both elements. For element B, $w = (\xi^2-1)(\xi-1)(1+\eta)/8$ and $\left(\frac{\partial w}{\partial y}\right) = \frac{l_{2-3}}{2}(\xi^2-1)(\xi-1)/8$ along side 2-5. The slope $\frac{\partial w}{\partial y}$ is therefore discontinuous along the common side. This indicates that the MZC element is incompatible (non-conforming) [ZT2,Ya].

The discontinuity in the slope orthogonal to a side, termed hereafter the *normal rotation* (Figure 5.10a) implies that the cross derivatives $\frac{\partial^2 w}{\partial x \partial y}$ and $\frac{\partial^2 w}{\partial y \partial x}$ take a different value at the nodes, and this violates one of the basic requirements for the continuity of w. Figure 5.10b shows that $\frac{\partial w}{\partial y}$ along side 1-2 depends on $\left(\frac{\partial w}{\partial y}\right)_1$ and $\left(\frac{\partial w}{\partial y}\right)_2$, whereas $\frac{\partial w}{\partial x}$ along side 2-3 depends on $\left(\frac{\partial w}{\partial x}\right)_2$ and $\left(\frac{\partial w}{\partial x}\right)_3$. Therefore, the derivative $\frac{\partial^2 w}{\partial x \partial y}$ along side 1-2 depends on $\left(\frac{\partial w}{\partial y}\right)_1$. Similarly $\frac{\partial^2 w}{\partial y \partial x}$ along side 2-3 depends on $\left(\frac{\partial w}{\partial x}\right)_3$. Generally $\left(\frac{\partial w}{\partial y}\right)_1$ and $\left(\frac{\partial w}{\partial x}\right)_3$ will take different values and obviously $\left(\frac{\partial^2 w}{\partial x \partial y}\right)_2 \neq \left(\frac{\partial^2 w}{\partial y \partial x}\right)_2$.

It is therefore imposible to guarantee the conformity of the MZC thin plate rectangle simply by taking the deflection and its first derivatives as nodal variables. This, however, does not invalidate the element which

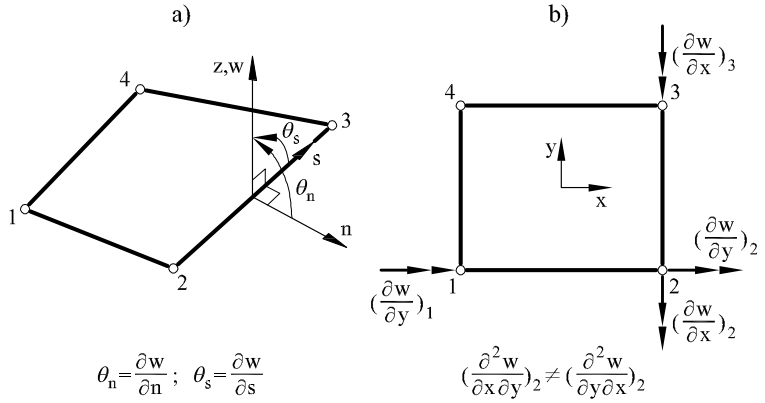

Fig. 5.10 (a) Normal (θ_n) and tangential (θ_s) rotations. (b) Discontinuity of $\frac{\partial^2 w}{\partial x \partial y}$ at node 2

satisfies the patch test (Section 5.9) [TZSC,Ya,ZTZ]. This ensures the convergence as the mesh is refined.

Unfortunately the patch test is not satisfied for arbitrary quadrilateral shapes as the constant curvature criterion is violated in those situations. This *limits the application of the MZC element plate domains that can be discretized into rectangular plate elements*. However, in these cases it is an accurate element, as shown in the examples presented below.

Henshell *et al.* [HWW] studied the performance of the MZC thin plate element (and also some other plate quadrilaterals of higher order) formulated in curvilinear coordinates and concluded that reasonable accuracy is obtained for arbitrary quadrilateral shapes. The use of curvilinear coordinate for extending the MZC element to parallelogram shapes is discussed in [Da,ZCh,ZCh2,ZT2]. Argyris [Ar2] proposed a different approach for deriving the shape function of a similar 4-noded plate quadrilateral.

Example 5.2: Obtain the deflection and bending moment distributions along the central line of the homogeneous isotropic clamped plate shown in Figure 5.11 under uniformly distributed loading of intensity $f_z = -q$. Use a mesh of 2×2 MZC elements with $\nu = 0.3$.

- Solution

Only a quarter of the plate is analyzed due to the double symmetry of the problem. After eliminating the columns and rows of the prescribed nodal

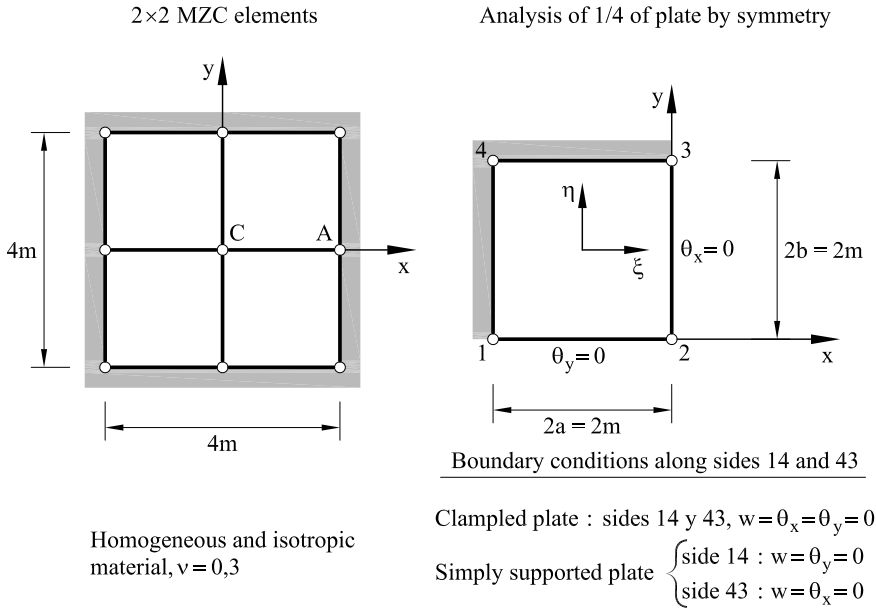

Fig. 5.11 Square plates analyzed with a mesh of 2×2 MZC thin plate rectangular elements

DOFs in the stiffness matrix of the single element considered and using the force vector of Eq.(5.47a), the following equation for the only free nodal variable, i.e. the deflection w_2, is obtained

$$\hat{d}_{11}\left[\frac{b}{a^3}+\frac{a}{b^3}+\frac{\nu}{2ab}+\frac{21(1-\nu)}{30ab}\right]w_2=-qab$$

Making $\nu = 0.3$ and $a = b = 1$ (Figure 5.11) gives

$$2.64\hat{d}_{11}w_2=-q$$

and

$$w_2=-0.378\frac{q}{D} \quad \text{with} \quad \hat{d}_{11}=\frac{Et^3}{12(1-\nu^2)}=D$$

The exact solution for this problem is (for $L = 4$) [TW]

$$w_2=-0.00126L^4\frac{q}{\hat{d}_{11}}=-0.322\frac{q}{D}$$

The error between the exact and computed deflections is $\approx 17\%$. The deflection field is obtained by substituting w_2 in the expression for w of Figure 5.8 to give

$$w=-0.0472\frac{q}{D}(1+\xi)(1-\eta)(2+\xi-\eta-\xi^2-\eta^2)$$

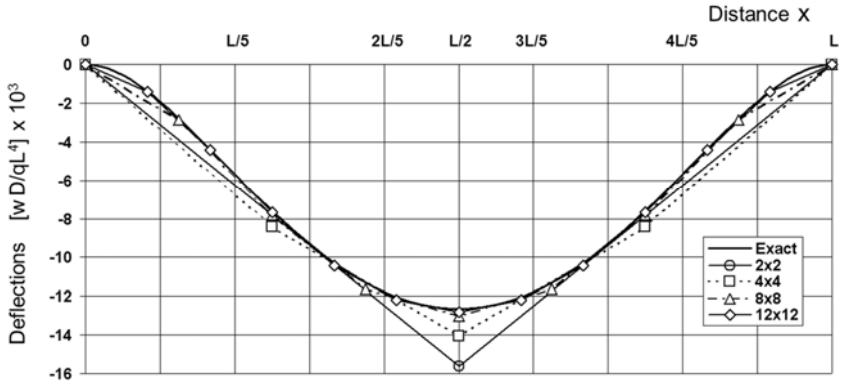

(a) w

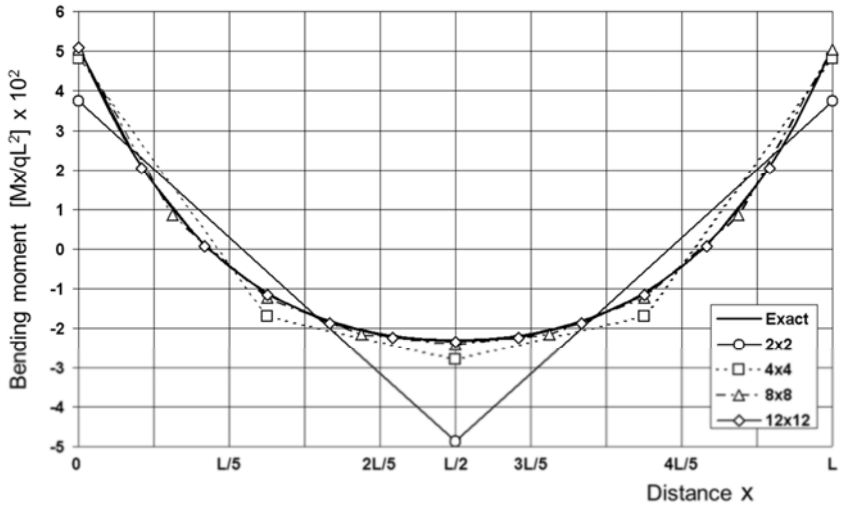

(b) M_x

Fig. 5.12 Clamped square plate under uniform loading. Deflection and bending moment (M_x) diagrams along the central line for meshes of 2×2, 4×4, 8×8 and 12×12 MZC elements

Along the central line ($\eta = -1$)

$$w = -0.0944 \frac{q}{D}(1+\xi)(2+\xi-\xi^2)$$

which is a cubic polynomial in ξ as expected. This solution is compared with the exact one [TW] in Figure 5.12a and also with that obtained using meshes of 2×2, 4×4 and 8×8 MZC elements. Note the excellent accuracy of the central deflection value obtained with the simple 2×2 mesh.

The bending moment distribution within the element is obtained from the value of w_2 and the expressions of Box 5.2 (with $\nu = 0.3$, $\hat{d}_{11} = \hat{d}_{22} = D$ and

$\hat{d}_{33} = \frac{1-\nu}{2} D = 0.35D$) giving

$$M_x = -\frac{3\hat{d}_{11}}{4a^2b^2}[\xi(1-\eta)b^2 - 0.3\eta(1+\xi)a^2]w_2 = -0.284q[\xi - 0.3\eta - 1.3\xi\eta]$$

$$M_y = -\frac{3\hat{d}_{11}}{4a^2b^2}[0.3\xi(1-\eta)b^2 - \eta(1+\xi)a^2]w_2 = -0.284q[0.3\xi - \eta - 1.3\xi\eta]$$

$$M_{xy} = -\frac{\hat{d}_{33}}{4ab}[3\xi^2 + 3\eta^2 - 4]w_2 = -0.034q[3\xi^2 + 3\eta^2 - 4]$$

The distribution of M_x and M_y along side 1-2 ($\eta = -1$) is linear in ξ whereas M_{xy} is quadratic. The linear distribution of M_x along the central line is compared in Figure 5.12b with the exact one [TW] and with that obtained using different meshes. The accuracy of the bending moment solution is poorer than that for the deflection, as expected. However, even for the coarse 4×4 mesh the values of M_x at the center and the clamped edge are a good estimate for design purposes.

The bending moments computed at the 2×2 Gauss points approximate better the exact values. This is further evidence of the benefit of computing the stresses at the "optimal sampling points" ([ZTZ] and Section 6.7 of [On4]).

Table 5.1 shows the percentage error values versus the exact solution of the deflection and the bending moment M_x at the plate center C and at the mid-point of the clamped edge (point A in Figure 5.11).

Figure 5.13 shows the convergence of the distribution of w and M_x along the central line for different meshes. We see that the MZC thin plate element element, although it is incompatible, converges in its rectangular form. Finally, Figure 5.14 shows the contours for w, M_x and M_y in one quarter of plate for a 14×14 mesh.

MCZ mesh	w_C	M_x^C	M_x^A
2×2	23,49%	112,77%	-11,52%
4×4	11,25%	22,17%	-2,63%
8×8	3,08%	4,99%	-0,79%
12×12	1,38%	2,17%	-0,39%
Analytical [TW]	$w_C = -0,00126\frac{qL^4}{D}$	$M_x^C = -2,291 \times 10^{-2} qL^2$	$M_x^A = -2,24 M_x^C$

Table 5.1 Deflection at plate center (C) and bending moment M_x at plate center (C) and the mid-point of clamped edge (A) for different meshes of MZC elements. Numbers show percentage error versus the analytical solution [TW]

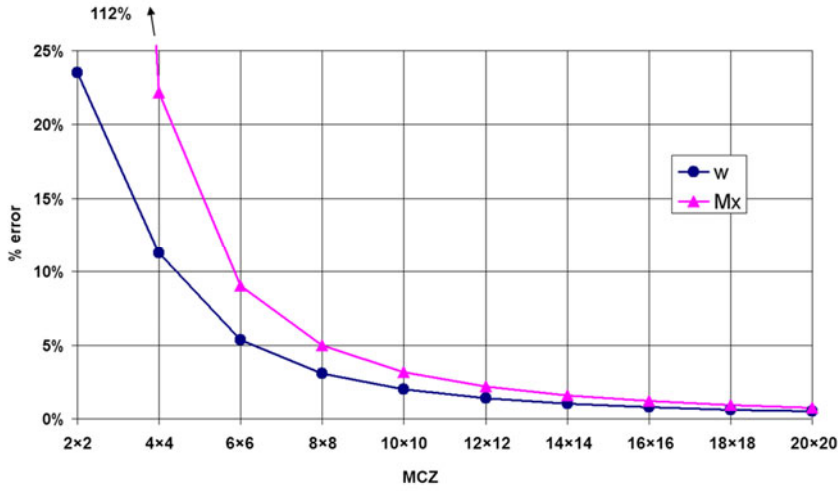

Fig. 5.13 Clamped square plate under uniform loading. Convergence of the error in the deflection w and the bending moment M_x at the central point for different meshes of MZC thin plate rectangles

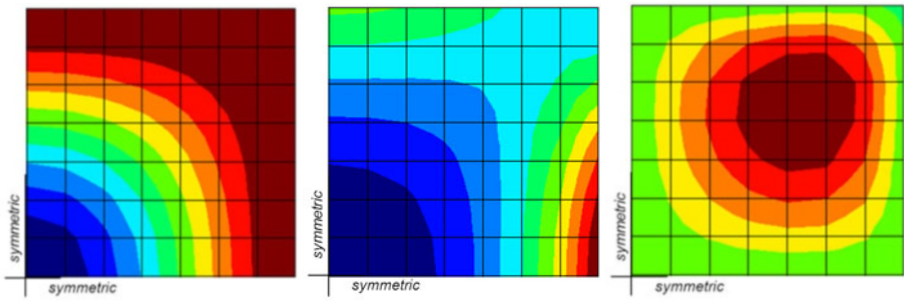

(a) w (b) M_x (c) M_{xy}

Fig. 5.14 Clamped square plate under uniform loading. Contours of vertical deflection w (a) and bending moments M_x (b) and M_{xy} (c) for a mesh of 14×14 MZC rectangles. Results are shown in one quarter of the plate due to symmetry

---

Example 5.3: Obtain the central deflection for the clamped plate of Figure 5.11 under a central point load $(-P)$. Use a mesh of 2×2 MZC elements.

- Solution

The process is identical to that followed in the previous example. The load acting at node 2 is $-\frac{P}{4}$ due to symmetry. The equation for w_2 is

$$2.64\hat{d}_{11}w_2 = -\frac{P}{4} \quad \text{and} \quad w_2 = \frac{-P}{10.56\hat{d}_{11}} = -0.0946\frac{P}{\hat{d}_{11}}$$

The error with respect to the analytical solution ($w_2 = -0.0896\frac{P}{\hat{d}_{11}}$ [TW]) is $\approx 5.5\%$. The bending moment distribution is obtained as in the previous example.

Example 5.4: Obtain the central deflection for the square plate of Figure 5.11 with simple supported edges under: a) Uniformly distributed loading ($-q$), and b) Central point load ($-P$) using a mesh of 2×2 MZC thin plate rectangular elements.

- Solution

Case a) Uniformly distributed loading

Along the simply supported sides 14 and 43 we just need to prescribe $w = 0$. This automatically implies $\theta_s = 0$ along these edges. Hence the only non-zero DOFs due to the double symmetry are θ_{x_1}, w_2 and θ_{y_3} (Figure 5.11). The resulting system of three equations is deduced as

$$\begin{gathered}\left(\frac{4b}{3a}+\frac{4(1-\nu)a}{15b}\right)\theta_{x_1}-\left(\frac{b}{a^2}+\frac{(1-\nu)}{10b}\right)w_2=-\frac{qab^2}{3D}\\ -\left(\frac{b}{a^2}+\frac{(1-\nu)}{10a}\right)\theta_{x_1}+\left(\frac{b}{a^3}+\frac{a}{b^3}+\frac{\nu}{2ab}+\frac{7(1-\nu)}{10ab}\right)w_2+\\ +\left(\frac{a}{b^2}+\frac{(1-\nu)}{10a}\right)\theta_{y_3}=-\frac{qab}{\hat{D}}\\ \left(\frac{a}{b^2}+\frac{(1-\nu)}{10a}\right)w_2+\left(\frac{4a}{3b}+\frac{4(1-\nu)b^2}{15ab}\right)\theta_{y_3}=\frac{qab^2}{3D}\end{gathered}$$

with $D = \hat{d}_{11}$.
Making $\nu = 0.3$ and $a = b = 1$ and noting that due to symmetry $\theta_{y_3} = -\theta_{x_1}$, the above system can be simplified to

$$\begin{gathered}1.52\theta_{x_1}-1.07w_2=-0.33\frac{q}{D}\\ -2.14\theta_{x_1}+2.64w_2=-\frac{q}{D}\end{gathered}$$

which gives

$$w_2 = -1.25\frac{q}{D} \quad \text{and} \quad \theta_{x_1} = -\theta_{x_3} = -1.08\frac{q}{D}$$

The bending moment distribution can be obtained from Box 5.2.
The value of w_2 agrees reasonably well with the exact one of $w_2 = -1.040\frac{q}{D}$ [TW] (error $\approx 20\%$) despite of the simplicity of the mesh.

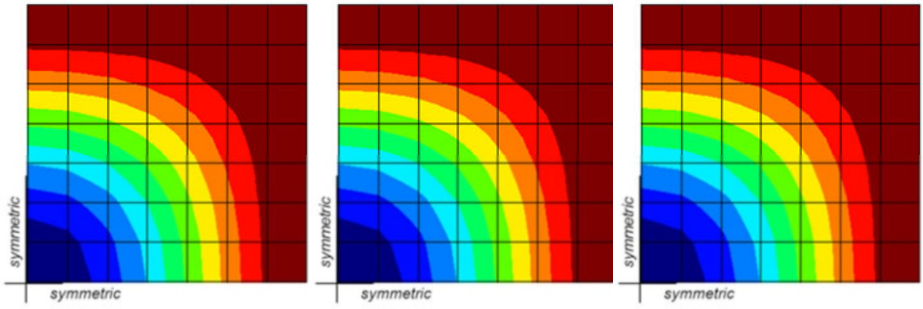

(a) w (b) M_x (c) M_{xy}

Fig. 5.15 Simple supported square plate. Uniform loading. Contours of vertical deflection (a) and bending moments M_x (b) and M_{xy} (c) for a mesh of 14×14 MZC rectangles. Results shown in one quarter of the plate due to symmetry

Figure 5.15 shows the contours of vertical deflection (a) and bending moments M_x (b) and M_{xy} (c) for a 14×14 mesh.

Case b) Central point load

The system of equations is the same as in the previous example substituting the 1st, 2nd and 3rd right-hand sides for $0, \frac{-P}{4D}$ and 0, respectively. After eliminating θ_{y_3} and making $\nu = 0.3$ and $a = b = 1$ we obtain

$$1.52\theta_{x_1} - 1.07w_2 = 0$$
$$-2.14\theta_{x_1} + 2.64w_2 = 0.33\frac{P}{D}$$

giving

$$w_2 = -0.219\frac{P}{D} \quad \text{and} \quad \theta_{x_1} = -\theta_{y_3} = -0.154\frac{P}{D}$$

The value of w_2 obtained with this very simple mesh is again not far from the analytical value, $w_2 = -0.1856\frac{P}{D}$ [TW] (error $\approx 18\%$).
The bending moment distribution can be obtained from Box 5.2.

5.4.2 12 DOFs plate rectangle proposed by Melosh

A rectangular plate element with the same DOFs as the MZC rectangle was derived almost simultaneously by Melosh [Me,Me2]. The shape functions are obtained by combining the 1D Hermite polynomials used for the 2-noded Euler-Bernouilli beam element (Section 1.3.1) giving the

following interpolations for the deflection

$$
\begin{aligned}
w = {} & N_1(x)N_1(y)w_1 + N_2(x)N_1(y)w_2 + N_2(x)N_2(y)w_3 + \\
& + N_1(x)N_2(y)w_4 + \bar{N}_1(x)N_1(y)\left(\frac{\partial w}{\partial x}\right)_1 + \bar{N}_2(x)N_1(y)\left(\frac{\partial w}{\partial x}\right)_2 + \\
& + \bar{N}_2(x)N_2(y)\left(\frac{\partial w}{\partial x}\right)_3 + \bar{N}_1(x)N_2(y)\left(\frac{\partial w}{\partial x}\right)_4 + N_1(x)\bar{N}_1(y)\left(\frac{\partial w}{\partial x}\right)_1 + \\
& + N_2(x)\bar{N}_1(y)\left(\frac{\partial w}{\partial x}\right)_2 + N_2(x)\bar{N}_2(y)\left(\frac{\partial w}{\partial x}\right)_3 + N_1(x)\bar{N}_2(y)\left(\frac{\partial w}{\partial x}\right)_4
\end{aligned}
\tag{5.48}
$$

where N_i and $\bar{N}_i$ are the Hermite polynomials of Eq.(1.11a) written in cartesian coordinates and referred to each of the element sides.

This element satisfies the continuity requirements for the normal rotation along the sides. However, the approximation (5.48) does not contain the term $\alpha_6 xy$ and the element can not reproduce a constant torque strain $\left(\frac{\partial^2 w}{\partial x \partial y}\right)$ state and this violates the patch test. This problem does not occur for the MZC element, neither for the BFS one presented in the next section. Consequently, these elements are more reliable for practical purposes.

5.4.3 Conforming BFS plate rectangle

Many authors have attempted to derive conforming Kirchhoff thin plate elements which satisfy the continuity requirements for the normal rotation and the second cross derivative $\frac{\partial^2 w}{\partial x \partial y}$ along the sides. A popular technique is to introduce the cross derivative $\frac{\partial^2 w}{\partial x \partial y}$ as a fourth nodal variable (Figure 5.16). Bogner, Fox and Schmidt [BFS] proposed an element of this type using a 16 term polynomial expansion for w as a product of two complete cubic polynomials in x and y.

An interesting feature of the BFS element is that, as for the Melosh rectangle, the shape functions can be obtained by simple products of 1D cubic Hermite polynomials. The approximation for the deflection is therefore written as

$$
w^{(e)} = [\mathbf{N}_w, \mathbf{N}_{\theta_x}, \mathbf{N}_{\theta_y}, \mathbf{N}_\Gamma] \begin{Bmatrix} \mathbf{w} \\ \boldsymbol{\theta}_x \\ \boldsymbol{\theta}_y \\ \boldsymbol{\Gamma} \end{Bmatrix} \tag{5.49}
$$

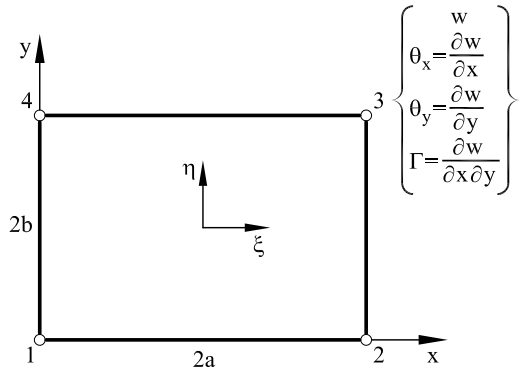

Fig. 5.16 4-noded conforming BFS plate rectangle

with

$$\mathbf{w} = [w_1, \ldots, w_4]^T; \qquad \boldsymbol{\theta}_x = \left[\left(\frac{\partial w}{\partial x}\right)_1, \ldots, \left(\frac{\partial w}{\partial x}\right)_4\right]^T$$
$$\boldsymbol{\theta}_y = \left[\left(\frac{\partial w}{\partial y}\right)_1, \ldots, \left(\frac{\partial w}{\partial y}\right)_4\right]^T; \quad \boldsymbol{\Gamma} = \left[\left(\frac{\partial w}{\partial x \partial y}\right)_1, \ldots, \left(\frac{\partial w}{\partial x \partial y}\right)_4\right]^T \tag{5.50}$$

and

$$\begin{aligned} N_{w_i} &= N_i(\xi), N_i(\eta) \quad , \quad N_{\theta_{xi}} = \bar{N}_i(\xi), N_i(\eta) \\ N_{\theta_{yi}} &= N_i(\xi), \bar{N}_i(\eta) \quad , \quad N_{\Gamma_i} = \bar{N}_i(\xi), \bar{N}_i(\eta) \end{aligned} \tag{5.51}$$

where N_i and $\bar{N}_i$ are the 1D Hermite shape functions of Eq.(1.11a).

Eqs.(5.50) and (5.51) allow the element stiffness matrix to be derived in a straightforward manner. Details can be found in [WJ,Ya]. The BFS element satisfies the continuity requirements for the normal and cross-derivatives along the sides. The reason is that the normal rotation varies along a side as a cubic polynomial uniquely defined by four parameters, i.e. one rotation and the cross derivative at each of the two end nodes. The element is therefore conforming and it satisfies the patch test. The BFS rectangle is more accurate than the MZC one [WJ]. This is not due to the conformity of the former, but to the fact that the BFS rectangle involves a higher approximation with more nodal variables.

Unfortunately, the practical use of the BFS element is limited to rectangular shapes only. The continuity requirements for the second cross derivatives at the nodes in arbitrary quadrilaterals requires all the second

derivatives of w with respect to the different side directions meeting at each node to be defined as nodal variable. Obviously this is quite difficult to generalize for practical purposes.

A development of the BFS element to include the continuity of higher derivatives was outlined in [Sp].

The derivation of conforming plate quadrilaterals starting from triangular plate elements will be studied in Section 5.6.

5.5 TRIANGULAR THIN PLATE ELEMENTS

Triangular plate elements are of interest for the analysis of plates with irregular shapes. Their formulation, however, has the same difficulties for satisfying conformity as the rectangular elements previously studied. Some of the more popular non-conforming and conforming Kirchhoff plate triangles are presented next.

5.5.1 Non-conforming thin plate triangles

Let us consider first the 3-noded triangle. The obvious choice of nodal variables gives a total of nine DOFs (w_i, $\left(\frac{\partial w}{\partial x}\right)_i$ and $\left(\frac{\partial w}{\partial y}\right)_i$ at each node). A complete cubic polynomial has ten terms and, hence, a problem arises when choosing the term to be dropped out. A number of authors have proposed different elements on the basis of the term omitted. Unfortunately all of them require substantial manipulation for ensuring conformity.

Adini and Clough [AC] omitted the xy term in the cubic expansion, i.e.

$$w(x,y) = a_1+a_2x+a_3y+a_4x^2+a_6y^2+a_7x^3+a_8x^2y+a_9xy^2+a_{10}y^3 \quad (5.52)$$

This simple criterion yields a poor element which is unable to reproduce constant torsion curvature $\left(\frac{\partial^2 w}{\partial x \partial y}\right)$ states. In addition, the element does not satisfy the C^1 continuity requirement.

Tocher and Kapur [TK] grouped the terms a_8 and a_9 of the cubic polynomial as

$$\begin{aligned} w(x,y) = a_1 + a_2x + a_3y + a_4x^2 + a_5xy + a_6y^2 + \\ +a_7x^3 + a_8(x^2y + xy^2) + a_9y^3 \end{aligned} \quad (5.53)$$

This element does not respect the continuity of the normal rotation along the sides. Also, matrix $\mathbf{A}$ of Eq.(5.33b) becomes singular when the sides of the triangle are parallel to the x, y axes [TK,To].

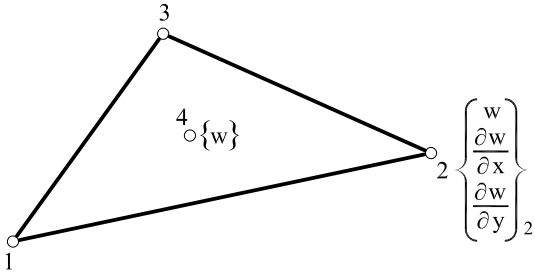

Fig. 5.17 4-noded plate triangle with 10 degrees of freedom [HK]

Harvey and Kelsey [HK] obtained a complete cubic deflection field by adding a fourth central node with a single deflection variable (Figure 5.17). The internal DOF can be eliminated by static condensation. The resulting element does not satisfy the continuity requirement for the normal rotation and it has poor convergence. The performance of this element can be substantially improved by imposing the continuity requirement using Lagrange multipliers. Harvey and Kelsey [HK] showed that the enhanced element satisfies the patch test and it converges monotonically to the exact solution. Further details can be found in [Ya].

Bazeley *et al.* [BCIZ] developed a 3-noded plate triangle with 9 DOFs. The element was subsequently modified by Cheung, King and Zienkiewicz [CKZ] (termed hereafter CKZ element). The starting point is an incomplete cubic expansion of the deflection using area coordinates as

$$w = a_1L_1 + a_2L_2 + a_3L_3 + a_4\left(L_1^2L_2 + \frac{L_1L_2L_3}{2}\right) + a_5\left(L_2^2L_1 + \frac{L_1L_2L_3}{2}\right)$$
$$+a_6\left(L_2^2L_3 + \frac{L_1L_2L_3}{2}\right) + a_7\left(L_3^2L_2 + \frac{L_1L_2L_3}{2}\right) +$$
$$+a_8\left(L_3^2L_1 + \frac{L_1L_2L_3}{2}\right) + a_9\left(L_1^2L_3 + \frac{L_1L_2L_3}{2}\right) \tag{5.54}$$

The bracketed terms guarantee the reproduction of an arbitrary curvature field (including that of constant curvature) for a zero value of the nodal deflections.

Following a similar procedure as for the MZC rectangle, Eq.(5.54) can be written in the form

$$w = \sum_{i=1}^{3}\left(N_iw_i + \bar{N}_i\left(\frac{\partial w}{\partial x}\right)_i + \bar{\bar{N}}_i\left(\frac{\partial w}{\partial y}\right)_i\right) \tag{5.55}$$

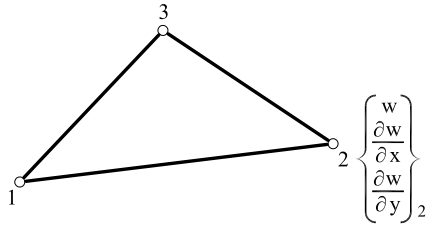

Shape functions :

$$N_1 = L_1 + L_1^2 L_2 + L_1^3 L_3 - L_1 L_2^2 - L_1 L_3^2 \qquad \bar{\bar{N}}_2 = b_1(L_2^2 L_3 + L) - b_3(L_1 L_2^2 + L)$$
$$\bar{N}_1 = c_3(L_1^2 L_2 + L) - c_2(L_3 L_1^2 + L) \qquad N_3 = L_3 + L_3^2 L_1 + L_3^2 L_2 - L_3 L_1^2 - L_3 L_2^2$$
$$\bar{\bar{N}}_1 = b_3(L_1^2 L_2 + L) - b_2(L_3 L_1^2 + L) \qquad \bar{N}_3 = c_2(L_3^2 L_1 + L) - c_1(L_2 L_3^2 + L)$$
$$N_2 = L_2 + L_2^2 L_3 + L_2^2 L_1 - L_2 L_3^2 - L_2 L_1^2 \qquad \bar{\bar{N}}_3 = b_2(L_3^2 L_1 + L) - b_1(L_2 L_3^2 + L)$$
$$\bar{N}_2 = c_1(L_2^2 L_3 + L) - c_3(L_1 L_2^2 + L)$$

$$L = \frac{L_1 L_2 L_3}{2} \qquad b_i = y_j - y_m \qquad c_i = x_m - x_j$$

Fig. 5.18 Shape functions for the 3-noded CKZ plate triangle [CKZ]

The shape functions N_i , $\bar{N}_i$ and $\bar{\bar{N}}_i$ are given in Figure 5.18. The stiffness matrix for this element can be found in [CKZ].

The CKZ triangle violates the continuity requirement for the normal rotation and hence is non conforming. However, it converges in a monotonic manner and this has contributed to its popularity [CKZ].

Bazeley *et al.* [BCIZ] proposed a correction to the deflection field leading to a linear distribution of the normal rotation along the sides. This modification does not improve the CKZ element substantially and the performance of the original form is sometimes superior.

Different authors have tried to enhance the behaviour of the CKZ triangle so that it passes the patch test [BN,FB2,KA]. A simple proposal was due to Specht [Sp] who achieved conformity by adding 4th degree terms to the cubic expansion (5.54) as

$$\begin{aligned} w = {} & a_1 L_1 + a_2 L_2 + a_3 L_3 + a_4 L_1 L_2 + a_5 L_2 L_3 + a_6 L_1 L_3 + \\ & + a_7 \left[L_1^2 L_2 + \frac{L}{2}(3(1-\gamma_3)) L_1 - (1+3\gamma_3) L_2 + (1+3\gamma_3) L_3 \right] + \\ & + a_8 \left[L_2^2 L_3 + \frac{L}{2}(3(1-\gamma_1)) L_2 - (1+3\gamma_1) L_3 + (1+3\gamma_1) L_1 \right] + \\ & + a_9 \left[L_3^2 L_1 + \frac{L}{2}(3(1-\gamma_2)) L_3 - (1+3\gamma_2) L_1 + (1+3\gamma_2) L_2 \right] \end{aligned} \tag{5.56}$$

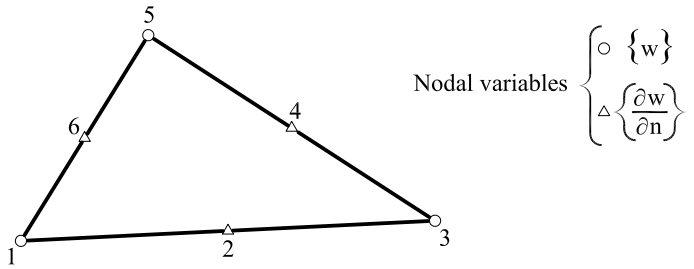

Fig. 5.19 Morley plate triangle of constant curvature

with $L = L_1 L_2 L_3$, $\gamma_1 = \frac{l_3^2 - l_2^2}{l_1^2}$; $\gamma_2 = \frac{l_1^2 - l_3^2}{l_2^2}$; $\gamma_3 = \frac{l_2^2 - l_1^2}{l_3^2}$ and l_1, l_2 and l_3 are the element sides. The element passes all patch tests and performs excellently [Sp,TZSC,ZT2].

Morley 6 DOFs constant curvature triangle

Morley proposed a simple non-conforming 6-noded triangle with just 6 DOFs [Mo,Mo2]. The element uses a complete quadratic expansion of the deflection in terms of the three corner deflection values and the three normal rotations at the mid-sides (Figure 5.19). The Morley triangle has constant curvature and bending moment fields. It satisfies the patch test and converges despite the violation of the C^1 continuity requirement, which demands a cubic deflection field. The element stiffness can be explicitly obtained by

$$\mathbf{K}^{(e)} = A^{(e)} \mathbf{B}^T \mathbf{D}_b \mathbf{B} \tag{5.57}$$

with

$$\mathbf{B} = \frac{1}{A^{(e)}} [\mathbf{G}_1, \mathbf{G}_2] \tag{5.58a}$$

$$\mathbf{G}_1 = -\begin{bmatrix} C_4 S_4 - C_6 S_6 & C_5 S_5 - C_4 S_4 & C_6 S_6 - C_5 S_5 \\ -C_4 S_4 + C_6 S_6 & -C_5 S_5 + C_4 S_4 & -C_6 S_6 + C_5 S_5 \\ -C_4^2 + S_4^2 + C_6^2 - S_6^2 & -C_5^2 + S_5^2 + C_4^2 - S_4^2 & -C_6^2 + S_6^2 + C_5^2 S_5^2 \end{bmatrix} \tag{5.58b}$$

$$\mathbf{G}_2 = \left[\mathbf{G}_2^4, \mathbf{G}_2^5, \mathbf{G}_2^6\right] \quad , \quad \mathbf{G}_2^k = -\begin{bmatrix} C_k^2 l_k \\ S_k^2 l_k \\ 2 S_k C_k l_k \end{bmatrix} \quad , \quad k = 4, 5, 6 \tag{5.58c}$$

where $C_k = y_{ji}/l_k$, $S_k = -x_{ji}/l_k$, $x_{ji} = x_j - x_i$, $y_{ji} = y_j - y_i$ and $l_k = (x_{ji}^2 + y_{ji}^2)^{1/2}$ is the lengh of side k. The constant bending moment field is

given by

$$\hat{\boldsymbol{\sigma}}_b = \mathbf{D}_b \mathbf{B} \mathbf{a}^{(e)} \tag{5.59a}$$

with

$$\mathbf{a}^{(e)} = \left[w_1, w_2, w_3, \left(\frac{\partial w}{\partial n}\right)_4, \left(\frac{\partial w}{\partial n}\right)_5, \left(\frac{\partial w}{\partial n}\right)_6 \right]^T \tag{5.59b}$$

The equivalent nodal force vector due to a uniformly distributed loading $f_z = q$ is

$$\mathbf{f}^{(e)} = q \frac{A^{(e)}}{3} [1, 1, 1, 0, 0, 0]^T \tag{5.60}$$

Nodal point loads are assumed to act at the corner nodes only. Full details on the derivation of the Morley triangle can be found in [Wo].

The Morley triangle is so far the simplest Kirchhoff plate triangle involving deflections and rotations as variables. Its simplicity is comparable to that of the constant strain triangle for plane elasticity problems. Despite its slow convergence, the Morley triangle enjoys big popularity for analysis of plates and shells. A thin plate triangle with identical features as the Morley triangle can be derived starting from the Reissner-Mindlin TLLL triangle (Section 6.8.3) using a Discrete Kirchhoff approach (see Section 6.8.3).

5.5.2 Conforming thin plate triangles

Satisfying the conformity requirements in triangles is a challenging task. The technique of using the curvatures as additional nodal variables is cumbersome and it also makes the extension of the elements for shell analysis difficult. A more successful alternative is to guarantee the continuity of the normal rotation along the sides using additional mid-side variables. Some of these elements are described next.

A conforming plate triangle emerges as a modification of the CKZ element previously described. The shape functions of Eq.(5.54) define a quadratic variation of the normal rotation along each side which can not be uniquely described by the two end values. A solution to this problem is adding three additional mid-side variables which coincide with the normal rotation to each side (Figure 5.20) [ZT]. This suffices to define a complete cubic variation of $\frac{\partial w}{\partial n}$ along each side and conformity is thus satisfied.

Clough and Tocher [CT] developed another conforming triangle starting from an idea of Hsieh in correspondence with Clough [Ya] (denoted here as HCT element). The shape functions are obtained by dividing the element into three inner triangular subdomains as shown in Figure 5.21a.

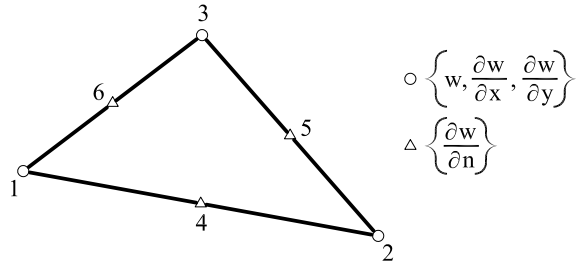

Fig. 5.20 Conforming 12 DOFs triangle

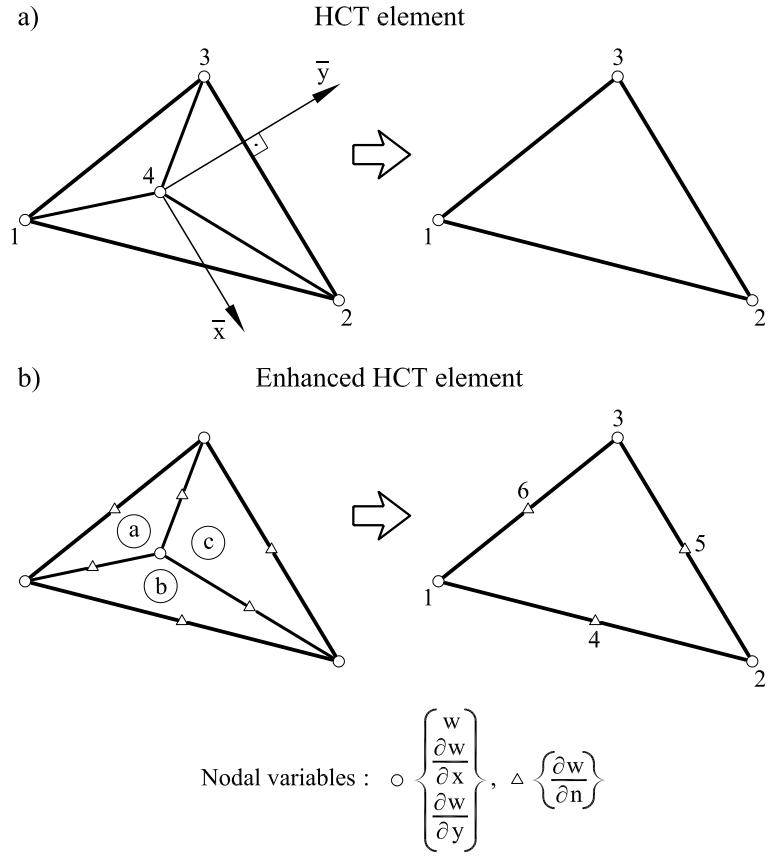

Fig. 5.21 HCT conforming thin plate triangles

A nine-term incomplete cubic expansion is written in the local axes $\bar{x}$, $\bar{y}$ for every triangular subdomain $4ij$ with $\bar{y}$ chosen orthogonal to the side ij. Thus, for the triangle 423 (Figure 5.21) we write

$$w_A = C_1 + C_2\bar{x} + C_3\bar{y} + C_4\bar{x}^2 + C_5\bar{y}^2 + C_6\bar{x}\bar{y} + C_7\bar{x}^3 + C_8\bar{x}\bar{y}^2 + C_9\bar{y}^3 \quad (5.61)$$

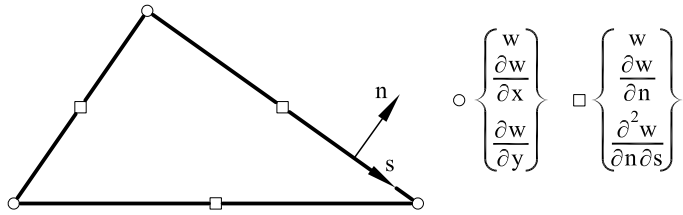

Fig. 5.22 18 DOFs conforming plate triangle proposed by Irons [Ir]

with $\bar{y}$ being orthogonal to side 23. Similar expressions are used for triangles 412 and 431. The omission of the term $\bar{x}^2\bar{y}$ in Eq.(5.61) guarantees that the normal rotation varies linearly along the external sides, whereas the deflection varies quadratically. The local stiffness matrices for each triangular subdomain are transformed to global axes for assembly purposes. The three DOFs of the central node are eliminated by imposing continuity of the normal rotation at the mid-point of the inner sides (three conditions). Further details can be found in [CMPW,CT,Ya]. The HCT element is conforming and it has 9 DOFs as the CKZ element. However, it has a slightly stiffer behaviour.

The performance of the HCT element can be enhanced by starting from three triangular subdomains where, in addition to the standard corner variables, a normal rotation variable is introduced at each mid-side point. This defines a quadratic variation of the rotation along the sides. After eliminating the internal variables a 12 DOFs plate triangle similar to the modified CKZ element is obtained (Figure 5.18b) [Ga2].

A drawback of elements with mid-side normal rotations as variables is that they involve a different number of DOFs per node. To overcome this problem Irons [Ir] proposed a 18 DOFs quartic triangle where the deflection and the curvature $\frac{\partial^2 w}{\partial n \partial s}$ are added as mid-side variables (Figure 5.22).

Other authors have proposed different 3-noded conforming plate triangles based on cubic and quartic expansions of the normal rotation $\frac{\partial w}{\partial n}$ along the sides. Cowper *et al.* [CKLO] proposed a 18 DOFs plate triangle with w, $\frac{\partial w}{\partial x}$, $\frac{\partial w}{\partial y}$, $\frac{\partial^2 w}{\partial x^2}$, $\frac{\partial^2 w}{\partial y^2}$, $\frac{\partial^2 w}{\partial x \partial y}$ at each node (Figure 5.23a). The shape functions omit three terms of a complete quintic polynomial (which has 21 terms) preserving a cubic variation of $\frac{\partial w}{\partial n}$ along the three sides.

This element can be enhanced by adding three mid-side nodes with the normal rotation as variable [AFS,Be,Ir] (Figure 5.23b). The shape

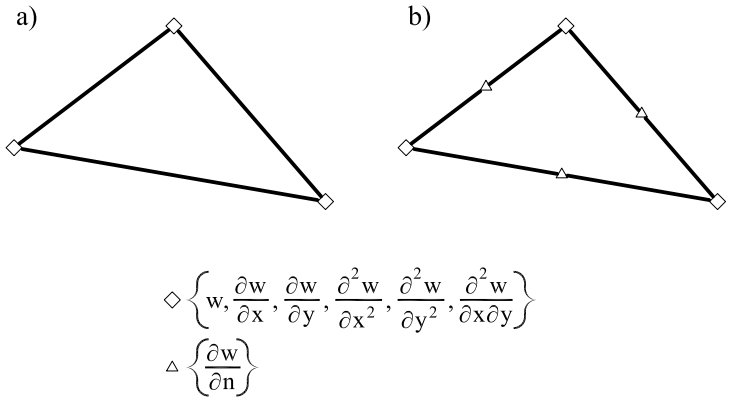

Fig. 5.23 18 and 21 DOFs conforming plate triangles

functions are now complete quintic polynomials (21 terms) and $\frac{\partial w}{\partial n}$ has a quartic variation along the sides.

More information on these elements can be found in [Ya,ZT2] in addition to the previously quoted references. Despite their accuracy, the practical acceptance of thin plate triangles with curvatures as nodal variables has been limited. The main reason for this is the intrinsic difficulties for their extension to shell analysis.

5.6 CONFORMING THIN PLATE QUADRILATERALS OBTAINED FROM TRIANGLES

One of the first conforming plate quadrilaterals derived from triangles is due to Fraejis de Veubeke [FdV,FdV2]. The element was later developed by Sander [San]. The starting point is the splitting of the quadrilateral into four inner triangles as shown in Figure 5.24a. A complete 10-term cubic polynomial is used to approximate the deflection within each subdomain and, thus, the total number of initial variables is 40. After eliminating the internal variables the DOFs are reduced to 16, i.e. the three standard corner variables and the normal rotations at the mid-side points. The element is conforming and it can be distorted to arbitrary quadrilateral shapes. The mid-side normal rotations are eliminated by imposing a linear variation of $\frac{\partial w}{\partial n}$ along each side. This, however, does not improve the performance of the element [FdV2].

A second thin plate quadrilateral was developed by Clough and Felippa [CF] almost at the same time as the Fraejis de Veubeke element described

a) Conforming quadrilateral of Fraeijs de Veubeke [FdV2]

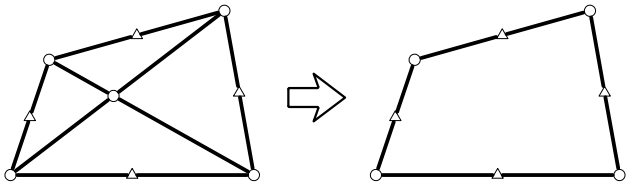

b) Conforming quadrilateral of Clough and Felippa [CF]

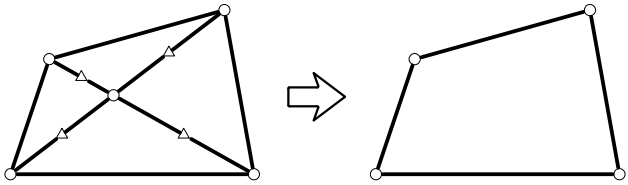

$$\text{Nodal variables}: \quad \circ \left\{ \begin{matrix} \mathrm{w} \\ \dfrac{\partial \mathrm{w}}{\partial \mathrm{x}} \\ \dfrac{\partial \mathrm{w}}{\partial \mathrm{y}} \end{matrix} \right\}, \quad \triangle \left\{ \dfrac{\partial \mathrm{w}}{\partial \mathrm{n}} \right\}$$

Fig. 5.24 Conforming plate quadrilaterals of Fraejis de Veubeke [FdV2] (a) and Clough and Felippa [CF] (b)

above. The triangular subdivision is very similar in both cases, as shown in Figure 5.24b. A complete cubic expansion is again used for the deflection within each inner triangle. All internal DOFs are eliminated after assembly by simple static condensation and also by imposing the continuity of the normal rotation at the internal mid-side nodes. The resulting conforming quadrilateral has only 12 DOFs and is quite accurate.

5.7 CONFORMING THIN PLATE ELEMENTS DERIVED FROM REISSNER-MINDLIN FORMULATION

Conforming thin plate elements can also be derived by "degeneration" of the C^o continuous Reissner-Mindlin plate elements to be studied in the next chapter. The process consists in constraining the transverse shear strains to take a zero value at a discrete number of points of the original Reissner-Mindlin element. Consequently, the "effective" shear energy is zero over the element. These elements are termed DK (for Discrete Kirch-

hoff) and they perform like Kirchhoff thin plate elements. However, *they only require C^o continuity for the displacement field* and this guarantees compatibility.

This technique can be considered as a generalization of that used in Chapter 2 for deriving Euler-Benouilli beam elements from Timoshenko elements (Section 2.8.4 and Examples 2.5 and 2.6).

The formulation of DK plate elements is described in the next chapter when dealing with Reissner–Mindlin thick plate theory. Nevertheless, we should keep in mind that they are another class of thin plate elements.

5.8 ROTATION-FREE THIN PLATE TRIANGLES

Rotation-free plate elements can be derived by extending the concepts explained in Section 1.4 for rotation-free Euler-Bernouilli beam elements.

The idea of using the deflection as the only nodal variable for plate bending analysis was originally exploited by finite difference (FD) practitioners [Ug]. The obvious difficulties in FD techniques are the treatment of boundary conditions and the problems when dealing with non-orthogonal or unstructured grids.

Several authors have proposed plate and shell finite elements with displacements as the nodal variables. Nay and Utku [NU] derived a rotation-free 3-noded thin plate triangle using a least square quadratic approximation to describe the deflection field within the patch surrounding a node in terms of the deflections of the patch nodes. The element stiffness matrix was obtained by the standard minimum potential energy approach. Later Barnes [Bar] proposed a method for deriving a 3-noded plate triangle with the nodal deflections as the only DOFs based on the computation of the curvatures in terms of the normal rotations at the mid-side points determined from the nodal deflections of adjacent elements. This method was exploited by Hampshire *et al.* [HTC] assuming that the elements are hinged together at their common boundaries, the bending stiffness being represented by torsional springs resisting the rotations about the hinge lines. Phaal and Calladine [PC2,3] presented a similar class of rotation-free triangles for plate and shell analysis. Yang *et al.* [YJS+] derived a family of triangular elements of this type for sheet stamping analysis based on so called bending energy augmented membrane approach which basically reproduces the hinge bending stiffness procedure described in [HTC]. Brunet and Sabourin [BS5,6,SB2] used a different method to compute the constant curvature field within each triangle in terms of the six nodal

displacements of a macro-element (quadrilateral). The triangle was successfully applied to non-linear shell analysis using an explicit dynamic approach. Rio *et al.* [RTL] have used the concept of side hinge bending stiffness for deriving a thin shell triangle of "translational" kind for explicit dynamic analysis of sheet stamping problems.

Oñate and Cervera [OC2] obtained a competititve and simple three node plate triangle with the deflection as the only nodal DOF by blending ideas from finite element and finite volume methods [IO,OCZ,ZO]. This work was generalized and extended by Oñate and Zarate [OZ] who used for the first time the name *rotation-free element* and derived two families of rotation-free plate and shell triangles by combining a standard linear finite element approximation over 3-noded triangles with cell centred (CC) and cell vertex (CV) finite volume schemes. These elements were extended to linear and non linear analysis of shells by Flores and Oñate [FO2,3,4] and Oñate *et al.* [OCM,OF,OFN]. Details of this two families of rotation-free plate triangles are given in the next sections.

Rotation-free thin plate and shell quadrilaterals have been derived by Savourin *et al.* [SCB2] and Flores and Estrada [FE]. These elements require some stabilization to avoid spurious deformation modes and are not so popular as the rotation-free triangles.

Other rotation-free plate and shell elements based on the upgrading of membrane theory to shells [LWB], isogeometric formulations [BBHH, KBLW] and Bezier interpolations over triangular patches [UO] have been recently proposed. Indeed, this topic seems to continue attracting much interest in the computational mechanics community.

5.8.1 Formulation of rotation-free triangles by a combined finite element and finite volume method

Let us consider an arbitrary discretization of the plate into standard 3-noded triangles. The curvature and the bending moments are described by constant fields within appropriate *non-overlapping control domains* (also termed "control volumes" in the finite volume literature [IO,OCZ,ZO]) covering the whole plate as

$$\hat{\boldsymbol{\varepsilon}}_b = \hat{\boldsymbol{\varepsilon}}_b^p \quad , \quad \hat{\boldsymbol{\sigma}}_b = \hat{\boldsymbol{\sigma}}_b^p \tag{5.62}$$

where $(\cdot)^p$ denotes constant values for the p-th control domain.

Two modalities of control domains are considered: a) that formed by a single triangular element (Figure 5.25a), and b) the control domain formed by one third of the areas of the elements surrounding a node (Figure

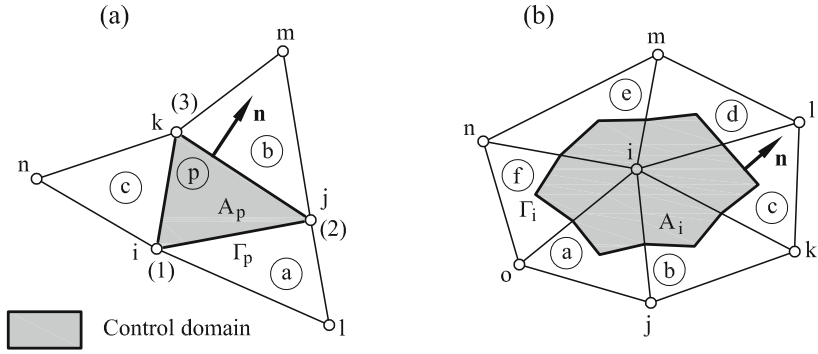

Fig. 5.25 Cell-centred (a) and cell-vertex (b) schemes. BPT and BPN triangles. Numbers in brackets denote local node numbers. Element sides are defined by opposite local node numbers, i.e. side 1 has nodes 2 and 3, etc.

5.25b). In the finite volume literature the two options are termed "cell-centred" (CC) and "cell-vertex" (CV) schemes, respectively [OCZ,ZO].

In the CC scheme each control domain coincides with a standard 3-noded finite element triangle. In the CV scheme a control domain is contributed by different elements, as shown in Figure 5.25b.

We identify the "patch of elements" associated with a control domain. In the CC scheme the patch is always formed by four elements (except in elements sharing a boundary segment). In the CV scheme the number of elements in the patch can vary.

In a CC scheme the chosen variables (i.e. the curvatures and bending moments) are "sampled" at the center of the cells discretizing the analysis domain (i.e. the 3-noded triangles). In a CV scheme the variables are sampled at the mesh nodes.

Let us now integrate the constitutive equation (5.14) and the curvature-deflection relationship (5.9) over each control domain as

$$\iint_{A_p} (\hat{\boldsymbol{\sigma}}_b - \hat{\mathbf{D}}_b \hat{\boldsymbol{\varepsilon}}_b) dA = 0 \tag{5.63}$$

$$\iint_{A_p} (\hat{\boldsymbol{\varepsilon}}_b - \mathbf{L}w) dA = 0 \tag{5.64}$$

where A_p is pth control domain area and the curvature operator $\mathbf{L}$ is

$$\mathbf{L} = \left[\frac{\partial^2}{\partial x^2}, \frac{\partial^2}{\partial y^2}, 2\frac{\partial^2}{\partial x \partial y} \right]^T \tag{5.65}$$

Eqs.(5.63) and (5.64) express the satisfaction of the constitutive and curvature-deflection equations over a control domain in a mean sense.

Introducing into Eq.(5.63) the assumed constant bending moment and curvature fields within each control domain gives

$$\hat{\boldsymbol{\sigma}}_b^p = \hat{\mathbf{D}}_b^p \hat{\boldsymbol{\varepsilon}}_b^p \quad , \quad \text{where} \quad \hat{\mathbf{D}}_b^p = \frac{1}{A_p} \iint_{A_p} \hat{\mathbf{D}}_b dA \tag{5.66}$$

is the average constitutive matrix over a control domain.

From Eqs.(5.62) and (5.64) we also obtain

$$\hat{\boldsymbol{\varepsilon}}_b^p = \frac{1}{A_p} \iint_{A_p} \mathbf{L} w \, dA \tag{5.67}$$

A simple integration by parts of the r.h.s. of Eq.(5.67) leads to

$$\boxed{\hat{\boldsymbol{\varepsilon}}_b^p = \frac{1}{A_p} \int_{\Gamma_p} \mathbf{T} \boldsymbol{\nabla} w d\Gamma} \tag{5.68}$$

where

$$\boldsymbol{\nabla} = \left[\frac{\partial}{\partial x}, \frac{\partial}{\partial y} \right]^T \quad , \quad \mathbf{T} = \begin{bmatrix} n_x & 0 & n_y \\ 0 & n_y & n_x \end{bmatrix}^T \tag{5.69a}$$

and n_x, n_y are the components of the outward unit normal $\mathbf{n}$ to the boundary Γ_p of the pth control domain (Figure 5.25). For the ith side of p with length l_i^p

$$\mathbf{n}_i = \frac{1}{l_i^p}[-b_i^p, -c_i^p] \quad , \quad \mathbf{T}_i = \frac{1}{l_i^p} \begin{bmatrix} b_i^p & 0 & c_i^p \\ 0 & c_i^p & b_i^p \end{bmatrix}^T \tag{5.69b}$$

$$b_i^p = y_j^p - y_k^p \quad , \quad c_i^p = x_k^p - x_j^p \quad i,j = 1,2,3 \tag{5.69c}$$

where parameters b_i^p and c_i^p are obtained by cyclic permutation of the indexes i, j, k.

Note that the element sides are defined by the opposite local node number, i.e. side 1 is defined by nodes 2,3, etc. (Figure 5.26).

Eq.(5.68) defines the average curvatures for each control volume in terms of the deflection gradients along its boundaries. The transformation of the area integral of Eq.(5.67) into the line integral of Eq.(5.68) is typical of finite volume methods [IO,OCZ,ZO].

The line integral in Eq.(5.68) poses a difficulty when the deflection gradient is discontinuous at the control domain boundary and some smoothing procedure is required. This issue is discussed below.

The PVW for the case of a distributed vertical load (Eq.(5.19)) is written as (noting that $\delta\hat{\boldsymbol{\varepsilon}}_b = \mathbf{L}\delta w$)

$$\sum_p \iint_{A_p} (\mathbf{L}\delta w)^T \hat{\boldsymbol{\sigma}}_b^p dA - \iint_A \delta w f_z dA = 0 \tag{5.70}$$

The sum in the first term of Eq.(5.70) extends over all the control domains in the mesh.

Integrating by parts the first integral in Eq.(5.70) and recalling that the bending moments are constant within each control domain, gives

$$\sum_p \left(\int_{\Gamma_p} [\mathbf{T}\boldsymbol{\nabla}\delta w]^T d\Gamma \right) \hat{\boldsymbol{\sigma}}_b^p - \iint_A \delta w f_z dA = 0 \tag{5.71}$$

Substituting Eqs.(5.66) and (5.68) into (5.71) yields finally

$$\sum_p \left\{ \left(\int_{\Gamma_p} [\mathbf{T}\boldsymbol{\nabla}\delta w]^T d\Gamma \right) \frac{1}{A_p} \hat{\mathbf{D}}_b^p \left(\int_{\Gamma_p} \mathbf{T}\boldsymbol{\nabla} w d\Gamma \right) \right\} - \iint_A \delta w f_z dA = 0 \tag{5.72}$$

Eq.(5.72) is the basis for deriving the final set of equilibrium equations, after the appropriate discretization of the deflection field.

An alternative derivation of Eq.(5.72) using a Hu-Washizu variational principle and a mixed formulation can be found in [OZ].

Derivation of the discretized equations

The deflection field is interpolated linearly within each triangular element in terms of the nodal values as in the standard FEM, i.e.

$$w = \sum_{i=1}^{3} N_i w_i = \mathbf{N}^{(e)} \mathbf{w}^{(e)} \tag{5.73}$$

with $\mathbf{N}^{(e)} = [N_1, N_2, N_3]$ and $\mathbf{w}^{(e)} = [w_1, w_2, w_3]^T$. In Eq.(5.73) N_i are the standard linear shape functions for the 3-noded triangle. Substituting Eq.(5.73) into (5.68) gives

$$\hat{\boldsymbol{\varepsilon}}_b^p = \frac{1}{A_p} \int_{\Gamma_p} \mathbf{T}\boldsymbol{\nabla}\mathbf{N}^{(e)} \mathbf{w}^{(e)} = \mathbf{B}^p \bar{\mathbf{w}}^p \tag{5.74}$$

where vector $\bar{\mathbf{w}}^p$ lists the deflections of the nodes linked to the p-th control domain and $\mathbf{B}^p$ is the curvature matrix relating the constant curvature field within each control domain and the nodal deflections $\bar{\mathbf{w}}^p$. Matrix $\mathbf{B}^p$ is different for the CC and CV schemes.

Substituting Eq.(5.73) into (5.72) and using (5.74) gives the final system of equilibrium equations as

$$\mathbf{K}\mathbf{w} = \mathbf{f} \tag{5.75}$$

where vector $\mathbf{w}$ contains the nodal deflections of all mesh nodes. The global stiffness matrix $\mathbf{K}$ is obtained by assembling in the usual manner the stiffness contributions from the different control domains given by

$$\mathbf{K}^p = [\mathbf{B}^p]^T \hat{\mathbf{D}}_b^p \mathbf{B}^p A_p \tag{5.76}$$

The components of the nodal force vector $\mathbf{f}$ in Eq.(5.75) are obtained as for standard C° linear finite element triangles [On4], i. e.

Point loads

$$f_i = P_{z_i} \tag{5.77}$$

where P_{z_i} is the vertical point load acting on the i-th node

Distributed loading

$$f_i^{(e)} = \iint_{A^{(e)}} N_i f_z(x) dA \tag{5.78}$$

The global nodal force component f_i is obtained by assembling the element contributions $f_i^{(e)}$. For a constant distributed load $f_z = q$

$$f_i = \sum_e \frac{qA^{(e)}}{3} \tag{5.79}$$

where the sum extends over all the triangles sharing the i-th node, and $A^{(e)}$ is the area of element e.

The previous equations are particularized next for CC and CV schemes.

5.8.2 Cell-centred patch. BPT rotation-free plate triangle

In CC patches the control domain coincides with an individual element and the evaluation of the constant curvature field of Eq.(5.68) can be simply written as

$$\hat{\boldsymbol{\varepsilon}}_b^p = \frac{1}{A_p} \sum_{j=1}^{3} l_j^p \mathbf{T}_j^p (\boldsymbol{\nabla} w)_j^p = \mathbf{C}_p (\overline{\boldsymbol{\nabla} w})^p \tag{5.80a}$$

with

$$\mathbf{C}_p = [\mathbf{C}_1^p, \mathbf{C}_2^p, \mathbf{C}_3^p] \quad , \quad \mathbf{C}_i^p = \frac{1}{l_i^p} \begin{bmatrix} b_i^p & 0 \\ 0 & c_i^p \\ c_i^p & 0 \end{bmatrix} \quad , \quad (\overline{\boldsymbol{\nabla} w})^p = \begin{Bmatrix} (\boldsymbol{\nabla} w)_1^p \\ (\boldsymbol{\nabla} w)_2^p \\ (\boldsymbol{\nabla} w)_3^p \end{Bmatrix} \tag{5.80b}$$

In Eq.(5.80a) the sum extends over the three sides of element p coinciding with the pth control domain, $\mathbf{T}_j^p$ is the transformation matrix of

Eq.(5.69) for the side j of element p, $(\boldsymbol{\nabla} w)_j^p$ is the deflection gradient at the side mid-point, x_j^p, y_j^p are the coordinates of node j of element p.

The evaluation of the deflection gradient $(\boldsymbol{\nabla} w)_i^p$ at the element sides in Eq.(5.80a) poses a difficulty as these gradients are discontinuous across elements for linear interpolations of w. Oñate and Cervera [OC2] overcome this problem by computing the deflection gradient at the triangle sides as the average values of the gradients contributed by the two elements sharing the side. This gives

$$(\overline{\boldsymbol{\nabla} w})^p = \mathbf{M}_p (\widehat{\boldsymbol{\nabla} w})^p \tag{5.81a}$$

with

$$\mathbf{M}_p = \frac{1}{2}\begin{bmatrix} \mathbf{I}_2 & \mathbf{0}_2 & \mathbf{I}_2 & \mathbf{0}_2 \\ \mathbf{I}_2 & \mathbf{0}_2 & \mathbf{0}_2 & \mathbf{I}_2 \\ \mathbf{I}_2 & \mathbf{I}_2 & \mathbf{0}_2 & \mathbf{0}_2 \end{bmatrix} \;,\; (\widehat{\boldsymbol{\nabla} w})^p = \begin{Bmatrix} (\boldsymbol{\nabla} w)^p \\ (\boldsymbol{\nabla} w)^a \\ (\boldsymbol{\nabla} w)^b \\ (\boldsymbol{\nabla} w)^c \end{Bmatrix} \;,\; \mathbf{I}_2 = \begin{bmatrix} 1 & 0 \\ 0 & 1 \end{bmatrix} \;,\; \mathbf{0}_2 = \begin{bmatrix} 0 & 0 \\ 0 & 0 \end{bmatrix} \tag{5.81b}$$

In Eq.(5.81b) $(\boldsymbol{\nabla} w)^k$ is the (constant) deflection gradient at element k.

Substituting the linear interpolation of the deflection (Eq.(5.73)) into (5.81a) gives

$$(\overline{\boldsymbol{\nabla} w})^p = \mathbf{M}_p \mathbf{G}_p \bar{\mathbf{w}}^p \tag{5.82}$$

with

$$\mathbf{G}_p = \begin{bmatrix} \bar{b}_1^p & \bar{b}_2^p & \bar{b}_3^p & 0 & 0 & 0 \\ \bar{c}_1^p & \bar{c}_2^p & \bar{c}_3^p & 0 & 0 & 0 \\ \bar{b}_3^a & \bar{b}_2^a & 0 & \bar{b}_1^a & 0 & 0 \\ \bar{c}_3^a & \bar{c}_2^a & 0 & \bar{c}_1^a & 0 & 0 \\ 0 & \bar{b}_3^b & \bar{b}_2^b & 0 & \bar{b}_1^b & 0 \\ 0 & \bar{c}_3^b & \bar{c}_2^b & 0 & \bar{c}_1^b & 0 \\ \bar{b}_2^c & 0 & \bar{b}_3^c & 0 & 0 & \bar{b}_1^c \\ \bar{c}_2^c & 0 & \bar{c}_3^c & 0 & 0 & \bar{c}_1^c \end{bmatrix} \quad , \quad \bar{\mathbf{w}}^p = \begin{Bmatrix} w_i \\ w_j \\ w_k \\ w_l \\ w_m \\ w_n \end{Bmatrix} \tag{5.83}$$

where $\bar{b}_i^p = \frac{b_i^p}{2A^p}$, $\bar{c}_i^p = \frac{c_i^p}{2A^p}$ with b_i^p, c_i^p given in Eq.(5.69c).

Substituting Eq.(5.82) into (5.80a) gives finally

$$\hat{\boldsymbol{\varepsilon}}_b^p = \mathbf{C}_p \mathbf{M}_p \mathbf{G}_p \bar{\mathbf{w}}^p = \mathbf{B}^p \bar{\mathbf{w}}^p \tag{5.84a}$$

with the curvature matrix $\mathbf{B}^p$ for element p given by

$$\mathbf{B}^p = \mathbf{C}_p \mathbf{M}_p \mathbf{G}_p \tag{5.84b}$$

$\mathbf{B}^p$ is a 3×6 matrix relating the curvatures with the deflections at the six nodes of the four element patch contributing to the control domain. Consequently, $\mathbf{K}^p$ is a 6×6 stiffness matrix.

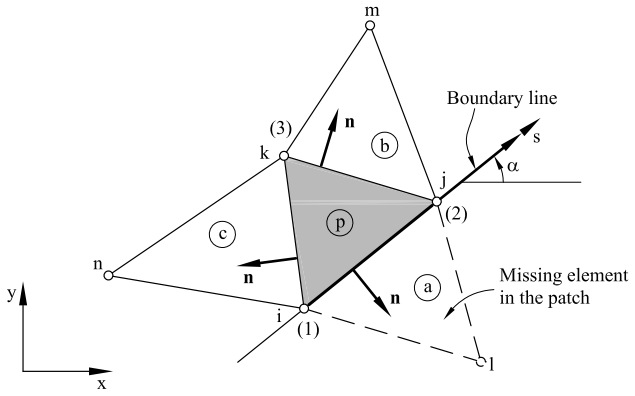

Side number	Nodes
1	2, 3
2	3, 1
3	1, 2

Fig. 5.26 Basic plate triangle (BPT) next to a boundary line. Numbers in brackets denote local node numbers. Definition of element sides

The resulting plate element is termed BPT (for Basic Plate Triangle). The element can be viewed as a standard finite element plate triangle with one DOF per node and a wider bandwidth, as each element is linked to its neighbours through Eq.(5.84a).

The BPT element can be extended to shell analysis leading to a simple and accurate rotation-free shell triangle (Section 8.13).

5.8.2.1 Boundary conditions for the BPT element

A difference between the BPT element and standard plate elements is that the conditions on the prescribed rotations must be imposed when building the curvature matrix $\mathbf{B}_p$.

Free edge

A BPT element with a side along a free boundary edge has one of the elements contributing to the patch missing. The contribution of this element is therefore omitted in matrix $\mathbf{M}^p$ of Eq.(5.81b) when performing the average of the deflection gradients. Thus, if side 3 corresponding to nodes i, j lies on a free boundary (Figure 5.26), matrix $\mathbf{M}^p$ is modified as

$$\mathbf{M}_p = \frac{1}{2}\begin{bmatrix} \mathbf{I}_2 & \mathbf{0}_2 & \mathbf{I}_2 & \mathbf{0}_2 \\ \mathbf{I}_2 & \mathbf{0}_2 & \mathbf{0}_2 & \mathbf{I}_2 \\ 2\mathbf{I}_2 & \mathbf{0}_2 & \mathbf{0}_2 & \mathbf{0}_2 \end{bmatrix} \tag{5.85}$$

while matrix $\mathbf{G}_p$ of Eq.(5.83) can remain unaltered. Clearly, the deflection at node 1 in the missing element should be prescribed to zero.

Additional conditions must be imposed on boundary edges where the rotations and/or the deflections are constrained as explained next.

Simply supported edge $\left(w = \dfrac{\partial w}{\partial s} = 0\right)$

The condition $\frac{\partial w}{\partial s} = 0$, where s is the boundary direction, is imposed by prescribing $w = 0$ at the boundary nodes. The "missing" element in the patch at the boundary edge is treated as described above for the free edge.

Clamped edge $(w = \boldsymbol{\nabla} w = 0)$

The condition $w = 0$ at clamped edges is satisfied by making the corresponding nodal deflections equal to zero when solving the global system of equations, as it is standard in the FEM.

The condition of zero rotations is imposed by disregarding the contributions from the clamped edges when computing the sum along the element sides in Eq.(5.80a). For instance, if side ij is clamped, matrix $\mathbf{M}_p$ of Eq.(5.81b) is modified as

$$\mathbf{M}_p = \frac{1}{2}\begin{bmatrix} \mathbf{I}_2 & \mathbf{0}_2 & \mathbf{I}_2 & \mathbf{0}_2 \\ \mathbf{I}_2 & \mathbf{0}_2 & \mathbf{0}_2 & \mathbf{I}_2 \\ \mathbf{0}_2 & \mathbf{0}_2 & \mathbf{0}_2 & \mathbf{0}_2 \end{bmatrix} \tag{5.86}$$

Symmetry line $\left(\dfrac{\partial w}{\partial n} = 0\right)$

The condition of zero normal rotation is imposed by neglecting the contribution from the prescribed rotation term at the symmetry line when computing Eq.(5.80a).

Let us assume that side 3 of element p with nodes i, j is a symmetry axis (Figure 5.26). The deflection gradient at that side is expressed in term of the tangential and normal rotations as

$$(\boldsymbol{\nabla} w)_3^p = \begin{bmatrix} C_\alpha & S_\alpha \\ S_\alpha & -C_\alpha \end{bmatrix} \begin{Bmatrix} \dfrac{\partial w}{\partial s} \\ \\ \dfrac{\partial w}{\partial n} \end{Bmatrix}_3^p \tag{5.87}$$

where s and n are the directions along the side and normal to the side, respectively, $C_\alpha = \cos\alpha$ and $S_\alpha = \sin\alpha$ and α is the angle that the side forms with the x axis (Figure 5.26).

The condition of zero normal rotation at the side is now introduced in Eq.(5.87), i.e.

$$(\boldsymbol{\nabla} w)_3^p = \begin{bmatrix} C_\alpha & S_\alpha \\ S_\alpha & C_\alpha \end{bmatrix} \begin{Bmatrix} \dfrac{w_j - w_i}{l_3^p} \\ 0 \end{Bmatrix} = \frac{1}{l_3^p} \begin{bmatrix} -C_\alpha & C_\alpha \\ -S_\alpha & S_\alpha \end{bmatrix} \begin{Bmatrix} w_i \\ w_j \end{Bmatrix} \tag{5.88}$$

Matrix $\mathbf{M}_p$ is modified to account for the contribution of the element adjacent to the side lying on the symmetry axis only as

$$\mathbf{M}_p = \frac{1}{2} \begin{bmatrix} \mathbf{I}_2 & \mathbf{0}_2 & \mathbf{I}_2 & \mathbf{0}_2 \\ \mathbf{I}_2 & \mathbf{0}_2 & \mathbf{0}_2 & \mathbf{I}_2 \\ \mathbf{0}_2 & 2\mathbf{I}_2 & \mathbf{0}_2 & \mathbf{0}_2 \end{bmatrix} \tag{5.89}$$

Finally, the third and four rows of matrix $\mathbf{G}_p$ are modified as

$$\frac{1}{l_3^p} \begin{bmatrix} -C_\alpha & C_\alpha & 0 & 0 & 0 & 0 \\ -S_\alpha & S_\alpha & 0 & 0 & 0 & 0 \end{bmatrix} \tag{5.90}$$

5.8.3 Cell-vertex patch. BPN rotation-free plate triangle

A different class of rotation-free plate triangles can be derived starting from the "cell vertex" (CV) scheme (Figure 5.25b) [OZ]. The advantage is that the deflection gradient is now continuous along the control domain boundary. This allows the constant curvature vector to be computed directly over the control domain as

$$\hat{\boldsymbol{\varepsilon}}_b^i = \frac{1}{A_i} \int_{\Gamma_i} \mathbf{T} \boldsymbol{\nabla} \mathbf{N}_i \boldsymbol{w}_i d\Gamma = \mathbf{B}_i \bar{\mathbf{w}}_i \tag{5.91}$$

where $\mathbf{N}_i$ contains the contributions of the shape functions from all the elements participating to the i-th nodal control domain. Eq.(5.91) can be rewritten taking into account that the deflection gradients are constant within each element, as

$$\hat{\boldsymbol{\varepsilon}}_b^i = \frac{1}{A_i} \sum_{j=1}^{n_i} \frac{l_j}{2} \mathbf{T}_j \boldsymbol{\nabla} \mathbf{N}^{(j)} \boldsymbol{w}^{(j)} = \mathbf{B}_i \bar{\mathbf{w}}^i \tag{5.92}$$

where the sum extends over the n_i elements contributing to the i-th control domain (for instance $n_i = 5$ in Figure 5.27), l_j is the external side of element j, $\mathbf{T}_j$ is the transformation matrix of Eq.(5.69) for side l_j, superindex j refers to element values and $A_i = \frac{1}{3} \sum_{k=1}^{n_i} A^{(k)}$ where $A^{(k)}$ is the area of element k.

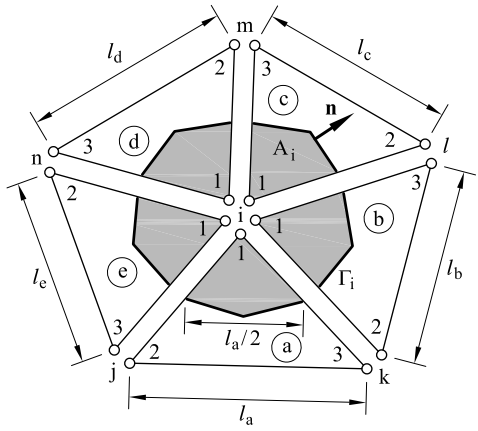

Fig. 5.27 BPN element. Typical CV control domain and numbering of nodes

Vector $\bar{\mathbf{w}}_i$ in Eq.(5.92) lists all the patch nodes. For instance in Figure 5.27, $\bar{\mathbf{w}}_i = [w_i, w_j, w_k, w_l, w_m, w_n]^T$.

The computation of the curvature matrix $\mathbf{B}_i$ for the patch is not so straightforward as its size depends on the number of nodes in the patch contributing to a nodal control domain. Typically,

$$\underset{3\times n}{\mathbf{B}_i} = \begin{matrix} 1 & 2 & \dots & n_p \\ \big[\mathbf{B}^i, & \mathbf{B}^a, & \dots, & \mathbf{B}^r\,\big] \end{matrix} \tag{5.93}$$

where n_p is the number of nodes in the patch (i.e. $n_p = 6$ for the patch of Figure 5.27) and upper indexes $i, a, \dots r$ refer to global node numbers. Box 5.3 shows matrix $\mathbf{B}_i$ for the control domain of Figure 5.27.

Note that $\mathbf{B}_i$ is the *global curvature matrix* for the central i-th node. The stiffness matrix for the i-th control domain is obtained as

$$\mathbf{K}_i = \mathbf{B}_i^T \hat{\mathbf{D}}_b^i \mathbf{B}_i \mathbf{A}_i \tag{5.94}$$

where $\hat{\mathbf{D}}_b^i$ is the average constitutive matrix for the i-th control domain. The global stiffness matrix is assembled from the nodal stiffness matrices $\mathbf{K}_i$ for the different control domains. The process is analogous to that followed for assembling the stiffness matrices for the CVB rotation-free beam element (Section 1.4.2). An element stiffness matrix can be also found by combining the nodal stiffness matrix of the three nodes as described for the CVB element. However, the direct assembly of the nodal stiffness matrix is recommended in practice.

$$\mathbf{B}_i = [\mathbf{B}^i, \mathbf{B}^j, \mathbf{B}^k, \mathbf{B}^l, \mathbf{B}^m, \mathbf{B}^n]$$

$$\mathbf{B}^i = \frac{1}{2A_i}[l_a \mathbf{T}_a \mathbf{G}_1^{(a)} + l_b \mathbf{T}_b \mathbf{G}_1^{(b)} + l_c \mathbf{T}_c \mathbf{G}_1^{(c)} + l_d \mathbf{T}_d \mathbf{G}_1^{(d)} + l_e \mathbf{T}_e \mathbf{G}_1^{(e)}]$$

$$\mathbf{B}^j = \frac{1}{2A_i}[l_a \mathbf{T}_a \mathbf{G}_2^{(a)} + l_e \mathbf{T}_e \mathbf{G}_3^{(e)}] \quad , \quad \mathbf{B}^k = \frac{1}{2A_i}[l_a \mathbf{T}_a \mathbf{G}_3^{(a)} + l_b \mathbf{T}_b \mathbf{G}_2^{(b)}]$$

$$\mathbf{B}^l = \frac{1}{2A_i}[l_b \mathbf{T}_b \mathbf{G}_3^{(b)} + l_c \mathbf{T}_c \mathbf{G}_2^{(c)}] \quad , \quad \mathbf{B}^m = \frac{1}{2A_i}[l_c \mathbf{T}_c \mathbf{G}_3^{(c)} + l_d \mathbf{T}_d \mathbf{G}_2^{(d)}]$$

$$\mathbf{B}^n = \frac{1}{2A_i}[l_d \mathbf{T}_d \mathbf{G}_3^{(d)} + l_e \mathbf{T}_e \mathbf{G}_2^{(e)}]$$

$$\mathbf{G}_i^{(k)} = \boldsymbol{\nabla} N_i^{(k)} = \frac{1}{2A^{(k)}} \begin{Bmatrix} b_i \\ c_i \end{Bmatrix}^{(k)} , \quad b_i^{(k)} = y_j^{(k)} - y_k^{(k)}, \quad c_i^{(k)} = x_k^{(k)} - x_j^{(k)}$$

Box 5.3 Curvature matrix for the BPN control domain of Figure 5.27

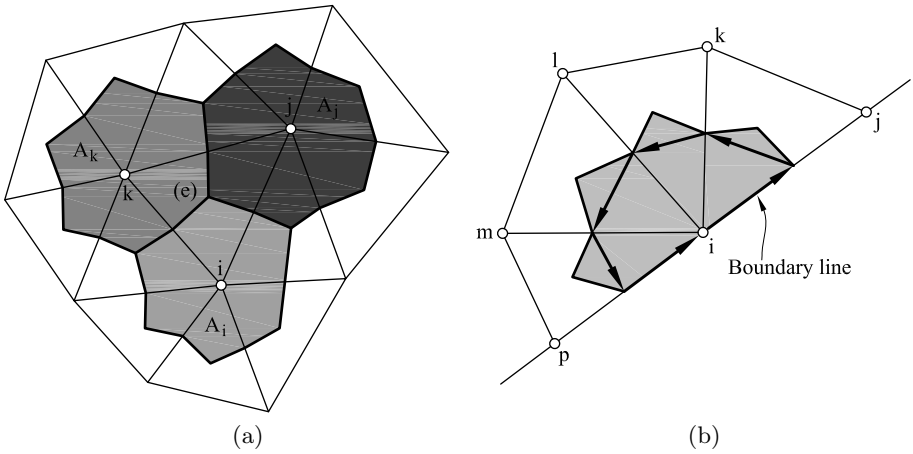

Fig. 5.28 (a) Contribution of control domains (in grey) to a rotation-free BPN triangle in the cell-vertex scheme. (b) Control domain sharing a boundary line. Arrows show the integration patch for computing the curvature matrix

The nodal force vector $\mathbf{f}_i$ is computed as explained in Section 5.8.1.

This plate element is termed BPN (for Basic Plate Nodal patch) [OZ]. The term "element" is somehow ambiguous as the BPN element combines a standard finite element interpolation over triangles with non-standard integration regions (the control domains) (Figure 5.28a).

The boundary conditions in the BPN element are imposed following the lines explained for the BPT element. The procedure is simpler as the deflection gradient is continuous on the control domain boundaries which lay within the elements. The conditions on the nodal deflections are imposed by prescribing w_i at the equations solution level. The conditions on the rotations, however, are imposed when building the curvature matrix. The integration patch for computing the curvature matrix should be adequately defined in this case. An example is shown in Figure 5.28b.

Clamped edges and symmetry lines. Zero rotations at clamped edges and symmetry lines are imposed by eliminating the contributions from these rotation terms in the sum of Eq.(5.92).

Simple supported edges. The condition $\frac{\partial w}{\partial s} = 0$ along an edge direction is accounted for by making zero the deflection at the edge nodes.

Free edges. No special treatment for the rotations is required at free edges. The performance of the element can be improved by prescribing the edge bending moments M_n and M_{sn} to a zero value. This can be simply done by making the appropriate rows in the constitutive matrix $\hat{\mathbf{D}}_b^p$ equal to zero at the patches containing a free edge. For free edges which are not parallel to one of the cartesian axes, a transformation of the constitutive equation to edge axes is necessary. This procedure can also be applied for prescribing the condition $M_n = 0$ at simply supported edges [OZ].

Similarly as for the CVB beam element (Section 1.4.3), the performance of the BPN element is superior to the BPT one for regular meshes. However, its accuracy slightly deteriorates for non-structured meshes and particularly when the control domains involve less than six nodes, since the evaluation of the curvatures is not as accurate in these cases. Also, its extension to shells is not so straightforward as for the BPT element.

5.9 PATCH TESTS FOR KIRCHHOFF PLATE ELEMENTS

The three modalities of patch tests A, B and C explained in Section 6.10 of [On4] are applicable to plate elements. Patch test A consists in prescribing a displacement field at all nodes of a patch of elements and checking that the equilibrium conditions are satisfied. In patch test B the displacements of the nodes at the boundary of the patch are prescribed. Then the values of the displacement at the internal nodes are computed and compared to the exact ones. Patch test C consists in assembling the matrix system for

the whole patch and finding the solution after fixing the minimum number of DOFs necessary to eliminate rigid body motion. The computed solution is then compared to the exact one. Satisfaction of patch tests A and B is a necessary conditions for convergence of the elements, while patch test C assesses the stability of the solution and provides a necessary and sufficient condition for convergence [On4,ZTZ].

A simple patch test of type B can be applied in thin plate elements in order to verify the good representation of rigid body displacements and the absence of spurious modes. The following displacement field is imposed at the boundary nodes

$$w = c - ax - by \tag{5.95}$$

where a, b and c are arbitrary numbers.

After solving the system of equations the internal DOFs must comply with Eq.(5.95) and the curvatures must be zero at each point in the patch.

A similar type B patch test can be devised for verifying the capability of the element for reproducing a constant curvature field. The test is based on imposing to the patch boundary nodes the quadratic displacement field

$$w(x, y) = \frac{1}{2}(ax^2 + by^2 + cxy) \tag{5.96}$$

where again a, b and c are arbitrary numbers. The numerical solution for the deflection at internal nodes must be in accordance with Eq.(5.96). Also, the curvature field must be constant at each point within the element giving $\hat{\boldsymbol{\varepsilon}}_b = [a, b, c]^T$.

For compatible Kirchhoff plate elements (i.e. those satisfying the C^1 continuity requirement) the patch tests are not theoretically needed. The tests however are useful for verifying the absence of programming errors.

5.10 COMPARISON OF KIRCHHOFF PLATE ELEMENTS

Some of the thin plate elements presented in this chapter are compared in the analysis of a clamped square plate under a central point load (Figure 5.29) and a uniformly distributed load (Figure 5.30). Only a quarter of the plate is discretized due to symmetry. Figures 5.29a and 5.30a show the error in the central deflection obtained with different meshes of rectangular elements. The non-conforming MZC element converges from above, thus giving an upper bound for the correct solution. This is so for most non-conforming elements. All the conforming elements considered converge from stiffer solutions in a fast and monotonic manner.

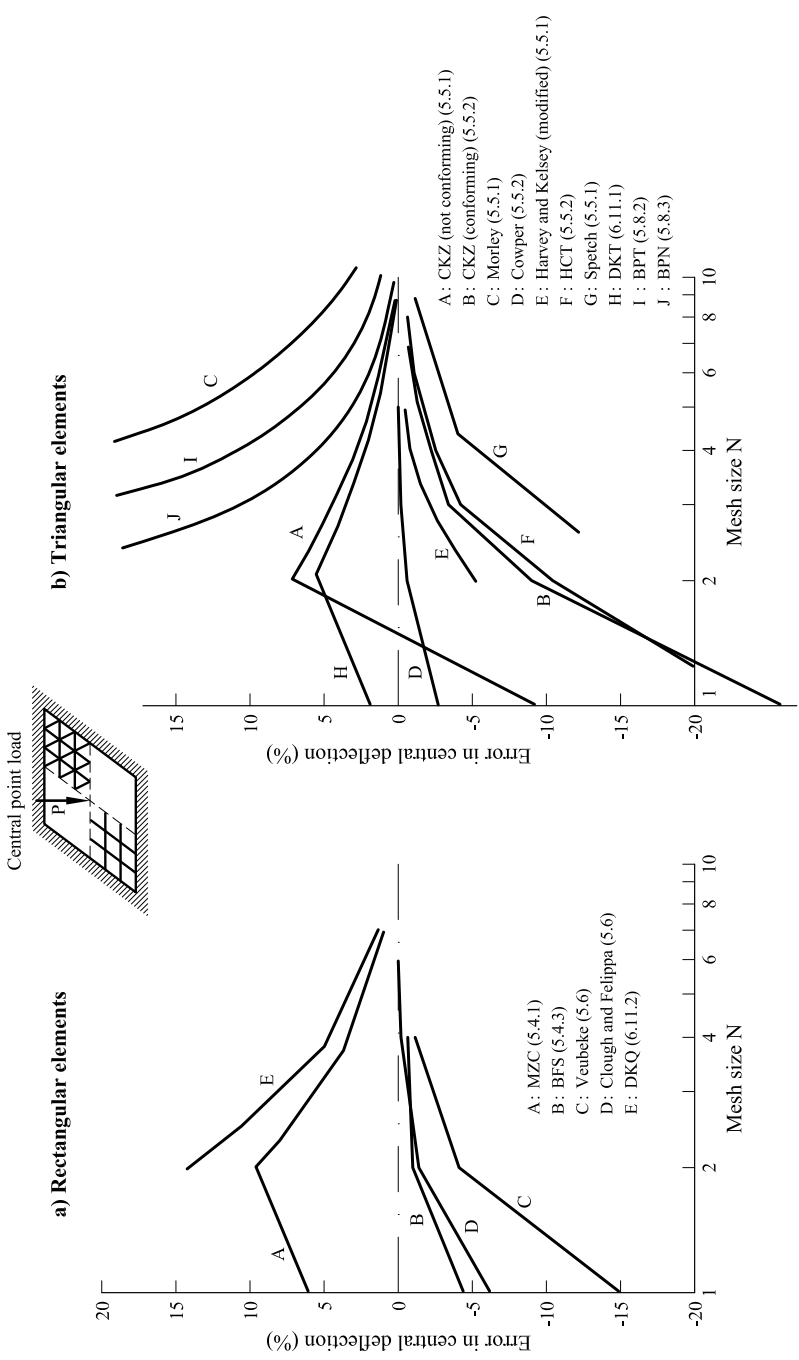

Fig. 5.29 Comparison of different rectangular and triangular Kirchhoff plate elements in the analysis of a clamped square plate under a central point load

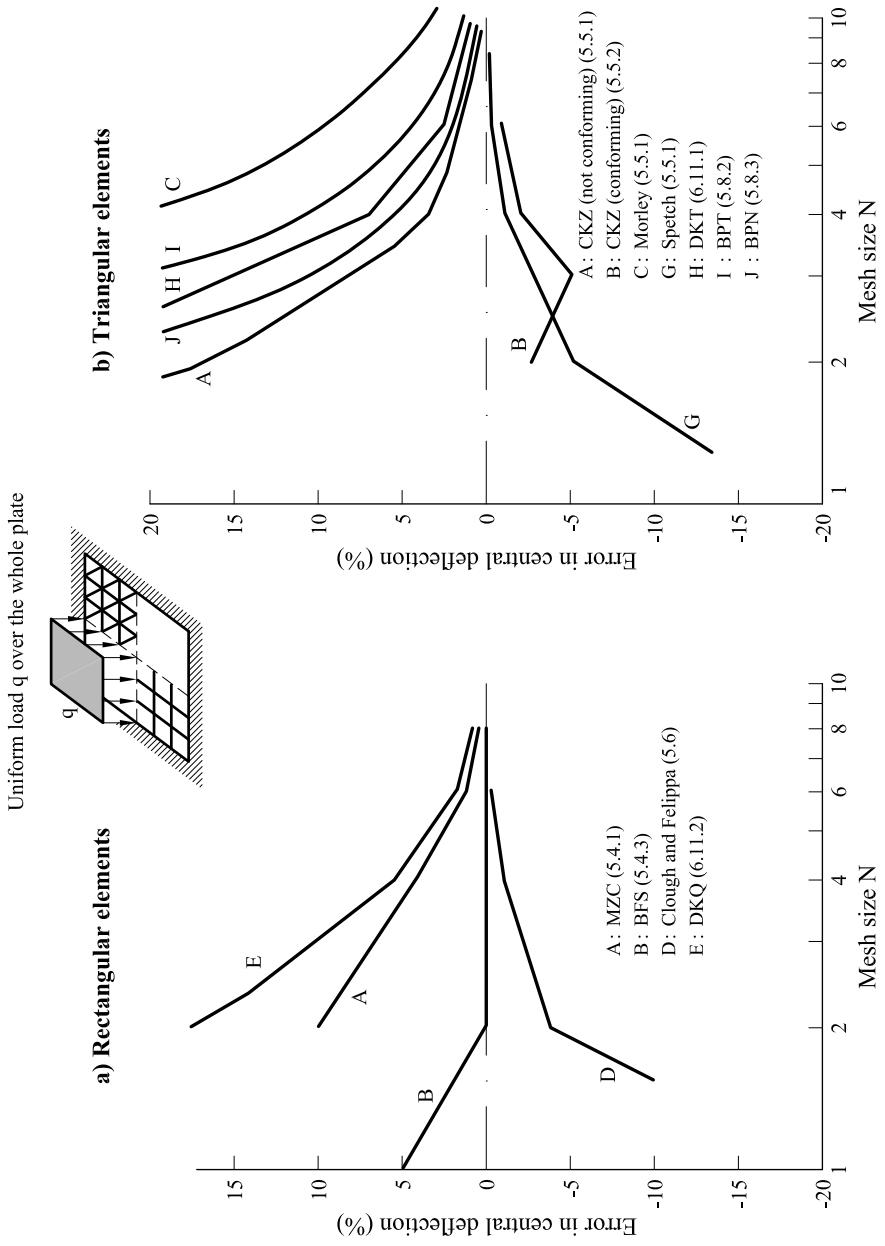

Fig. 5.30 Comparison of different rectangular and triangular Kirchhoff plate elements in the analysis of a clamped square plate under a uniformly distributed loading

The same type of analysis now using triangular elements is shown in Figures 5.29b and 5.30b. The solution for the Morley element is poor for coarse meshes as it involves fewer DOFs. Both the CKZ (non-conforming) and the Morley triangle elements converge from "the flexible side" due to their non-conformity. Conversely, the conforming triangles considered, i.e. Cooper *et al.* [CKLO], modified CKZ [ZT], HCT [CT] and Spetch [Sp] converge monotonically from the stiff side. The best results for coarse meshes were obtained with the first of these three elements. The modified 10 DOFs triangle of Harvey and Kelsey [HK] also converges to the exact solution. Very poor results (not shown in the figure) are found if the original version of this element is used. Note the monotonic convergence from the "flexible" side of the BST and BSN rotation-free triangles which *involve approximately one third of the DOFs* required for the rest of the elements tested. The good performance of the Discrete-Kirchhoff thin plate triangle (DKT) and quadrilateral (DKQ) described in Section 6.11 is also shown. The performance of all the element tested is very similar for simple supported plates.

More examples on the comparison of Kirchhoff plate elements can be found in [CMPW,Raz,SD,Ya,ZT2].

Abel and Desai [AD] assessed the "computational efficiency" of different Kirchhoff plate elements. This was defined as the computational effort required to obtain a prescribed accuracy and was measured in terms of the number of algebraic operations to solve the global equation system. The conclusion was that lower order elements are more efficient than higher order ones. Paradoxically, Rossow and Chen [RCh] arrived at the opposite conclusion simply by modifying the efficiency criterion and including the effect of the boundary conditions. The issue is therefore still open for discussion.

The advantage of higher order plate elements is their better ability to approximate complex bending moment fields over larger regions. Lower order elements are typically less accurate and require finer meshes. However, they usually include "physical" nodal variables (i.e. deflection and rotations) which avoids the cumbersome interpretation of the equivalent nodal force terms associated to higher order nodal variables, such as curvatures. Lower order triangular elements such as the Morley triangle and the BST and BSN rotation-free triangles are particularly attractive for practical applications and adaptive mesh refinement analysis.

5.11 CONCLUDING REMARKS

Kirchhoff thin plate theory requires C^1 continuity for the deflection field. This results in a higher complexity for deriving conforming plate elements that satisfy the C^1 continuity requirement.

Different conforming and non-conforming thin plate triangles and quadrilaterals have been studied and their behaviour has been compared in simple but illustrative examples of application.

A conclusion is that although conformity is not an essential requirement for the convergence of an element, it does guarantee a good performance for arbitrary geometries, and mainly for quadrilateral elements. Thus, any of the conforming quadrilaterals and triangles studied can be used with full confidence in practice. We note the simplicity of the MZC rectangle and the non-conforming Morley triangle which are two candidates for practical purposes.

The BPT and BPN rotation-free triangles have the deflection as the only nodal variable and their performance has been found to be very good for solving practical plate and shell problems [FO2,3,4,OCM,OF,OFN].

Kirchhoff plate elements based on mixed and hybrid formulations for which the displacements and the bending moments are simultaneously interpolated have not been studied in this chapter. Some successful elements of this type can be found in [ZT2]. A different family of plate elements is based on an explicit representation of the free strain states. This approach is called "natural formulation" in the thin plate and shell elements derived by Argyris *et al.* [AHM,AHMS,APAK,ATO,ATPA] and "free formulation" in the thin and thick elements proposed by Bergan *et al.* [BN,BW,FM]

In the next chapter we will derive an interesting family of Discrete-Kirchhoff thin plate elements starting from a "thick" (Reissner-Mindlin) plate formulation.